

# Human NLRC4 promotes cancer survival and is associated to Type-I Interferon signaling and immune infiltration

Charlotte Domblides<sup>1,2,3#</sup>, Steven Crampton<sup>4#</sup>, Hong Liu<sup>5#</sup>, Juliet M. Bartleson<sup>6</sup>, Annie Nguyen<sup>4</sup>, Claudia Champagne<sup>7</sup>, Emily E. Landy<sup>8</sup>, Lindsey Spiker<sup>9</sup>, Christopher Proffitt<sup>5</sup>, Sunil Bhattarai<sup>4</sup>, Anissa P. Grawe<sup>6</sup>, Matias Fuentealba Valenzuela<sup>6</sup>, Lydia Lartigue<sup>10</sup>, Isabelle Mahouche<sup>10</sup>, Jeremy Dupaul-Chicoine<sup>7</sup>, Kazuho Nishimura<sup>5</sup>, Félix Lefort<sup>2,3</sup>, Marie Decraecker<sup>2</sup>, Valérie Velasco<sup>11</sup>, Sonia Netzer<sup>1,2</sup>, Vincent Pitard<sup>1,2</sup>, Christian Roy<sup>5</sup>, Isabelle Soubeyran<sup>11</sup>, Victor Racine<sup>12</sup>, Patrick Blanco<sup>1,2</sup>, Julie Déchanet-Merville<sup>1,2</sup>, Maya Saleh<sup>13</sup>, Scott W. Canna<sup>14</sup>, David Furman<sup>6,15#\*</sup> and Benjamin Faustin<sup>1,2,4#\*</sup>

1. University of Bordeaux, 146 Rue Léo Saignat, 33076 Bordeaux, France.
2. ImmunoConcEpt, CNRS UMR 5164, INSERM ERL 1303, Bordeaux University, 33076 Bordeaux, France.
3. Department of Medical Oncology, University Hospital of Bordeaux, 33000 Bordeaux, France.
4. Immunology Discovery, Janssen Research and Development, 3210 Merryfield Row, San Diego, CA 92121, USA
5. GI and Immune-Oncology DDUs, Takeda Pharmaceuticals, San Diego CA, Cambridge, MA, USA
6. Buck Institute for Research on Aging, Novato, CA, USA
7. Department of Medicine, McGill University, Montreal, Qc, Canada
8. Department of Immunology, University of Pittsburgh School of Medicine, Pittsburgh, PA, USA
9. Department of Genetics, University of Pittsburgh School of Public Health, Pittsburgh, PA, USA
10. INSERM, U1218 ACTION, F-33000 Bordeaux, France.
11. Comprehensive Cancer Center, Department of Biopathology, Institut Bergonié, 33000 Bordeaux, France.
12. QuantaCell, Hôpital Saint Eloi, IRMB, 80 avenue Augustin Fliche, 34090 Montpellier, France
13. INRS Santé Biotechnologie, 531 Boulevard des prairies, Laval, Qc, Canada
14. Pediatric Rheumatology, The Children's Hospital of Philadelphia and University of Pennsylvania Perelman School of Medicine, Philadelphia, PA, USA
15. Stanford 1000 Immunomes Project, Stanford School of Medicine, Stanford CA 94305 USA

#Contributed equally

\*Address correspondence:

**Benjamin Faustin, PhD**

University of Bordeaux, CNRS UMR5164, ImmunoConcEpt  
146 Rue Léo Saignat, 33076 Bordeaux, France.  
email: [benfaustin@gmail.com](mailto:benfaustin@gmail.com)

**David Furman, PhD**

The Buck Institute for Research on Aging  
8001 Redwood Blvd, Novato, CA 94945  
email: [DFurman@buckinstitute.org](mailto:DFurman@buckinstitute.org), [furmand@stanford.edu](mailto:furmand@stanford.edu)

The authors have declared that no conflict of interest exists.

## **ABSTRACT**

The immune system can control cancer progression. However, even though some innate immune sensors of cellular stress are expressed intrinsically in epithelial cells, their potential role in cancer aggressiveness and subsequent overall survival in humans is mainly unknown. Here, we show that NLR family CARD Domain Containing 4 (NLRC4) is downregulated in epithelial tumor cells of colorectal cancer (CRC) patients by using spatial tissue imaging. Strikingly, only the loss of tumor NLRC4 but not stromal is associated with poor immune infiltration (mainly dendritic and CD4<sup>+</sup>/CD8<sup>+</sup> T cells) and accurately predicts progression to metastatic Stage IV and decrease of overall survival. By combining multi-omics approaches, we show that restoring NLRC4 expression in human colorectal cancer cells triggers a broad inflammasome-independent immune reprogramming consisting of Type-I IFN signaling genes and the release of chemokines and myeloid growth factors involved in the tumor infiltration and activation of dendritic cells (DCs) and T cells. Consistently, such reprogramming in cancer cells is sufficient to directly mature human DCs towards a Th1 antitumor immune response through IL-12 production *in vitro*. In multiple human carcinomas (colorectal, lung, and skin), we confirmed that *NLRC4* expression in patient tumors is strongly associated with Type-I IFN genes, immune infiltrates and high microsatellite instability. Thus, we shed light on the epithelial innate immune sensor NLRC4 as a novel therapeutic target to promote an efficient antitumor immune response against the aggressiveness of various carcinomas.

## INTRODUCTION

Higher vertebrates have developed innate protective mechanisms that can detect stress-induced cues triggered by infection, injury, or carcinogenesis. One example of cytosolic sensors of cellular perturbations are the nucleotide-binding domain and leucine-rich repeat (NLR) family of proteins. Some NLRs can be expressed in both epithelial and immune cells. After sensing cellular cues, NLRs assemble into a molecular scaffold that matures inflammatory caspases (including caspase-1) by a close-proximity mechanism. Such multi-protein complexes are called inflammasomes and depending on the specific NLR engaged in the machinery, distinct inflammasomes can form in response to a plethora of cellular insults (1). Active caspase-1 can then mediate numerous downstream immune signaling events including the maturation of inflammatory cytokine (IL-1 $\beta$  and IL-18), pyroptotic cell death, production of inflammatory lipids and modulation of cellular metabolism (1). NLR family CARD domain-containing 4 (NLRC4) is a crucial component of bacterial innate immune sensing by triggering diverse mechanisms involved in intestinal epithelial cell (IEC) homeostasis and innate immune responses through production of IL-18 among others after inflammasome formation (2). In addition to this role in pathogen sensing, NLRC4 function has recently expanded to trigger inflammation in sterile conditions through inflammasome assembly after the detection of metabolic dysregulation during aging and the presence of host short interspersed nuclear element (SINE) RNAs (3, 4).

Strikingly, in humans, constitutive NLRC4 hyperactivation through mendelian inheritance of various *de novo* gain-of-function (GOF) mutations display a broad array of clinical features including severe enterocolitis and gut inflammation (5–7), leading to autoinflammatory syndromes collectively termed as NLRC4 inflammasomopathies (8). A role for NLRC4 in the pathogenesis of cancer has also been proposed, albeit limited to studies relying on bulk tumor gene expression analysis and mouse models (9). Therefore, its relevance in human cancer and prognosis is scarce, including the critical cell-types involved and mechanism of protection. In

multiple colorectal cancer (CRC) patient cohorts, we show that loss of NLRC4 protein expression specifically in the tumor and not the stroma, is associated with aggressive metastatic progression, decreased patient survival and lower DC and T cell immune infiltrates. At the molecular level, we identified novel inflammasome-independent functions of NLRC4 in triggering Type-I IFN signaling and chemokine production in human colon cancer cells to directly mature DCs towards Th1 polarization *in vitro*. Hence, expression of human epithelial NLRC4 contributes to mounting an efficient antitumor immune response and protects against aggressive metastatic CRC and potentially others including lung and melanoma cancers.

## **RESULTS**

### **Loss of gut epithelial NLRC4 expression predicts poor clinical survival in colorectal cancer and progression to Stage IV metastasis**

To monitor protein expression levels in patient tumor cells and stroma, we utilized an immunofluorescence-based imaging approach using high-throughput analysis of Tissue MicroArrays (TMAs) with samples from healthy controls and patients diagnosed with various clinical stages of colorectal cancer (CRC). Samples were either collected from the Bergonié Cancer Institute or commercially sourced as a validation cohort (104 and 216 patients, respectively; clinical features of cohorts described in **Suppl. Table 1 and Suppl. Figure 2; see Methods**). The image-based epithelial segmentation of patient tissues used to determine protein levels of NLRC4, IL-1 $\beta$  and IL-18 expressed in epithelial cells versus stromal is described in **Suppl. Figure 1A and Methods**. **Suppl. Figure 1B** shows a robust loss of protein expression of NLRC4 as well as inflammasome-dependent cytokines IL-1 $\beta$  and IL-18 in tumor cells compared to normal tissue (104 patients, Bergonié cohort). Loss of NLRC4 was validated in an independent cohort of CRC patients (N=208, **Suppl. Figure 2**). This result is consistent with down-regulation of *NLRC4* gene expression obtained from TCGA transcriptomics analysis

of bulk tumors of patients with gastrointestinal cancer including colon adenocarcinoma (COAD), cholangiocarcinoma (CHOL), and liver hepatocellular carcinoma (LIHC) (**Suppl. Figure 1C, left**). Importantly, a strong down-regulation of *NLRC4* gene expression is also observed in patient tumors with lung cancers (adenocarcinoma LUAD, or squamous cell carcinoma LUSC) (**Suppl. Figure 1C, right**), hence, despite great variability among cancer types, the decrease of *NLRC4* in tumors seems to be a generalizable phenomenon. This analysis was extended to other epithelial-expressed NLR inflammasomes, and slightly different profiles were observed for *NLRP3*, *NLRP1* and *NLRP6*, with the most striking being for *AIM2* which down-regulation was only observed in LIHC (**Suppl. Figure 3 and 4**).

To address the clinical consequences of *NLRC4* expression in tumor tissues, the patients' cohort was stratified based on protein expression levels of *NLRC4*, IL-1 $\beta$ , or IL-18, as high versus low expression for each marker (above/below median; see **Suppl. Figure 5 and Methods**); either in the colon epithelium (within the cytokeratin mask) or in the stroma (outside the cytokeratin mask) (see Methods). Patients with high levels of *NLRC4* protein expression within the tumor had a better survival compared to those with low expression (HR: 0.44, 95IC: 0.22-0.79,  $p=0.0082$ ) (**Figure 1A, left**). The median overall survival was 56.98 months for *NLRC4*<sup>low</sup> patients (N=46), while the median was not reached for the *NLRC4*<sup>high</sup> individuals (N=58) within the study period. Variation of stromal *NLRC4* protein expression was not associated with a difference in overall survival (HR: 0.79, 95IC: 0.42-1.46,  $p=0.45$ ). In contrast to *NLRC4*, loss of IL-18 protein expression within both epithelial and stromal compartments was associated with a worse outcome ( $p=0.0004$ ). Interestingly, unlike *NLRC4* and IL-18, variation of IL-1 $\beta$  protein expression in the cytokeratin tumor mask was not associated with a difference in survival. Analysis of the independent ClinicalOutcome public dataset demonstrated improved survival in *NLRC4*<sup>high</sup> patients using tumor bulk analysis at the gene expression level from colon cancer patients ( $p=0.0169$ ) (**Suppl. Figure 6A**), as well as in lung cancers ( $p=0.0002$ )

**(Suppl. Figure 6B).** Improved survival of NLRC4<sup>normal</sup> patients was also observed for glioblastoma (p=0.0001), while other cancer types were not significant or missing data (**Suppl. Figure 6, Table**). Furthermore, consistent with the poor overall survival in NLRC4<sup>low</sup> expressing CRC tumors, compared to early clinical Stages I-II (N=44) and locally advanced Stage III cancer (N=37), a gradual loss of tumor NLRC4 protein expression was further observed in metastatic Stage IV cancer (N=23) (Stage I-II vs IV, p=0.0082) in our Bergonié cohort (**Figure 1A, right**). This was also the case for IL-18 (Stage I-II vs IV, p<0.0001), but not for IL-1 $\beta$  (**Figure 1A, right**). This loss of NLRC4 protein expression in aggressive Stage IV was further confirmed in the validation cohort (Stage I-II, N=150; Stage III, N=47; Stage IV=11) (**Suppl. Figure 2, below**). This loss of NLRC4 protein expression across tumor stages is consistent with a significant decrease at the gene expression level for COAD as well as lung cancers (LUAD and LUSC) (bulk tumor analysis from the TCGA patient dataset; **Suppl. Figure 7 A and B**). Therefore, gradual loss of NLRC4 protein expression in tumors, but not stromal cells, is associated with poor clinical survival of CRC patients, consistent with the aggressive progression to the metastatic stage. This observation might extend to human lung cancers as well.

To investigate this mechanism in mice, we used a genetically driven model of intestinal early polyp formation spontaneously occurring in *Apc*<sup>min/+</sup> mice (**see Methods**). In this model, high numbers of small intestine polyps were observed in *Apc*<sup>min/+</sup> mice, along with the loss of overall mucosal tissue architecture compared to healthy tissue (**Figure 1B**). Interrogation of mouse NLRC4 protein expression within the tumor (cytokeratin mask) showed a progressive loss of expression as the tumor grows between 3 and 6 months (**Figure 1C**). Consistently, it was shown that absence of NLRC4 expression in *Nlr4*<sup>-/-</sup> mice promotes colon tumorigenesis in the AOM/DSS-induced inflammatory colorectal cancer model wherein tumors appeared aggressive with invasion of tumor cells below the muscular mucosae (10). Therefore, the gradual loss of

NLRC4 expression in the tumor is associated with cancer progression and seems to be conserved between human and mouse.

### **Loss of tumor NLRC4 expression is associated with impaired T cell and DC immune infiltrates in cancer patients**

Based on its central role in the gut mucosal innate immune response, we hypothesized that NLRC4 may regulate the antitumor immune response in CRC patients. To test this, we interrogated immune infiltrates within tumors of our TMA cohort. We observed that compared to patients with high immune infiltrate (N=8), patients with low immune infiltrate (N=82) had concomitant lower expression of tumor NLRC4 ( $p=0.004$ ). This was more pronounced for total T cells ( $CD3^+$ ,  $p=0.006$ ), than in  $CD8^+$  T cells ( $p=0.03$ ) and was not significant for  $CD68^+$  and  $CD163^+$  macrophages (**Figure 2A**). To validate and extend this observation, we performed a TCGA cohort analysis to determine the abundance of additional tumor-infiltrating immune cell populations in COAD (9) (**Figure 2B**). Consistent with the results obtained from our TMAs, patients harboring *NLRC4*-null tumors (through genetic arm-level deletion) exhibited decreased  $CD4^+$  T cell tumor infiltration versus diploid normal tumors ( $p<0.01$ ). This was also true for neutrophils ( $p<0.01$ ) and even more significant for DCs ( $p<0.001$ ). Interestingly, this association of *NLRC4* with impaired infiltration of  $CD4^+$  T cells and DCs was not observed for *CASP1* nor *IL18* inflammasome genes (**Figure 2B**), and only for *IL1B* with DCs ( $p<0.01$ ) (**Suppl. Figure 8**). In addition, the level of *NLRC4* gene expression correlated strongly with immune infiltration of activated DCs (partial corr  $R=0.71$ ;  $p=2.2e-16$ ), and  $CD4^+$  and  $CD8^+$  T cells to a lesser extent (**Figure 2C**). To determine the prognostic relationship of both tumor NLRC4 and IL-18 protein expression combined, our TMAs of CRC patients were stratified according to the protein expression levels of NLRC4 and IL-18 as high versus low protein expression in epithelial cancer cells (**see Methods**).  $NLRC4^{low}/IL-18^{low}$  patients had a strong

decreased survival compared to NLRC4<sup>high</sup>/IL-18<sup>high</sup> individuals (HR: 0.26, 95IC: 0.09-0.45, p=0.0001) (**Figure 2D, left**). Median overall survival was 39.02 months for NLRC4<sup>low</sup>/IL-18<sup>low</sup> patients. Interestingly, there was no difference in overall survival between NLRC4<sup>high</sup>/IL-18<sup>high</sup> and NLRC4<sup>high</sup>/IL-18<sup>low</sup> patients (p=0.13) (**Figure 2D, middle**). Consistent with these results, the loss of IL-18 with preserved NLRC4 tumor expression (NLRC4<sup>high</sup>/IL-18<sup>low</sup>) was associated with an intermediate survival in comparison with either NLRC4<sup>high</sup>/IL-18<sup>high</sup> or NLRC4<sup>low</sup>/IL-18<sup>low</sup> patients (5-year survival rates of 82% for NLRC4<sup>high</sup>/IL-18<sup>high</sup>, 62% for NLRC4<sup>high</sup>/IL-18<sup>low</sup> and 35% for NLRC4<sup>low</sup>/IL-18<sup>low</sup>) (**Figure 2D, right**). These results suggest that part of the prognostic effect of NLRC4 tumor expression might involve IL-18 inflammasome-independent mechanisms. To test this, we investigated the effect of these stratifications on immune and T cell infiltrations in our TMAs (**Figure 2E**). Consistent with analysis on overall survival, NLRC4<sup>low</sup>/IL-18<sup>low</sup> patients were characterized by a decrease of mild and high immune infiltrates compared to the NLRC4<sup>high</sup>/IL-18<sup>high</sup> population, including CD3<sup>+</sup> and CD8<sup>+</sup> T cells. Importantly, no difference of immune infiltration was observed between NLRC4<sup>high</sup>/IL-18<sup>high</sup> and NLRC4<sup>high</sup>/IL-18<sup>low</sup> populations and the loss of NLRC4 tumor expression within the IL-18<sup>low</sup> population reduced mild infiltration to low level of both CD3<sup>+</sup> and CD8<sup>+</sup> T cells in tumors (~20% in frequency, respectively). Therefore, altogether, high tumor NLRC4 expression tracks with immune infiltration, including DCs and T cells, independently of tumor IL-18 variation, and this is consistent with better clinical survival of patients.

### **NLRC4 expression in human cancer cells mediates a Type-I IFN reprogramming, and is associated with high microsatellite instability in patient tumors**

To better define the NLRC4 inflammasome-independent mechanisms underlying survival of patients, we stably expressed NLRC4 in colon and monocytic cancer cell lines and conducted whole-genome transcriptomics analysis by RNAseq (**Figure 3A; Suppl Figure 9A and B; see**

**Methods).** As a control, NLRC4-mcherry expression in THP1 cell line versus mcherry control did not induce inflammasome activation as measured by IL-1 $\beta$  cytokine secretion, whereas strong release was triggered by Needle treatment (a specific trigger of the human NAIP/NLRC4 inflammasome) as expected (**Suppl. Figure 9C**). HT29-NLRC4 cell line did not display any changes in cell proliferation or migration compared to mock control (**Suppl. Figure 9D**). Compared to control, overexpression of NLRC4 in colon HT29 cells induced transcriptional up-regulation of 102 genes and down-regulation of 127 genes, while 102 genes were up-regulated and 144 down-regulated in THP1-NLRC4 monocytic cells (based on 2 FC cut-off,  $p < 0.05$ ) (**Figure 3A, left**). Among those, around a third were immune-related genes up-regulated in both cell lines (**Figure 3A, right**). KEGG pathway analysis of significant upregulated genes identified ‘Type-I interferon signaling pathway’ as the most significant pathway commonly induced in both cell lines (**Figure 3B**). **Figure 3C** illustrates the gene composition of this pathway in both NLRC4-expressing cell lines. Expression of Type-I IFN genes induced by NLRC4 was further confirmed in human primary monocytes by using mRNA transfections of NLRC4 GOF mutations (previously shown to induce constitutive activation). Both NLRC4 (T337S) and NLRP3 (R260W) neo-transcripts were expressed (**Figure 3D, left**), leading to upregulation of the top Type-I IFN genes (*CXCL10*, *DDX58*, *IFIT3*, *IFNA2*) commonly identified previously in NLRC4 stable cell lines (**Figure 3D, middle and right**). Upregulation of these genes were observed in response to NLRC4 (T337S) but not NLRP3 (R260W) GOF mutations. We also confirmed the upregulation of Type-I genes *IFNA2* and *IFNBI* using another NLRC4 GOF mutation (V341A), in contrast again to NLRP3 (R260W) GOF (**Suppl. Figure 10, bottom**) whereas both neo-transcripts were expressed and functional to induce Caspase-1 activity and IL-18 secretion as expected (**Suppl. Figure 10, top and middle**). Remarkably, the caspase-1 inhibitor YVAD had no effect on NLRC4 (V341A)-mediated increase of *IFNA2* and *IFNBI* gene expression (**Suppl. Figure 10, bottom**).

Consistent with these results obtained with NLRC4 (T337S) mRNA transfections in human primary monocytes, the induction of a broad Type-I IFN gene signature (encompassing 28 genes validated in patients with IFN-mediated diseases describe in 11) was further confirmed in THP1-NLRC4 (T337)-expressing stable cell line versus WT NLRC4 (**Suppl. Figure 11A**). These Type-I IFN stimulated genes were confirmed to be also upregulated in NLRC4 (T337S) patient monocytes versus healthy controls, but not in NLRP3 (G569R) patient monocytes (**Suppl. Figure 11B**). Unbiased gene set enrichment analysis of RNAseq revealed a top enrichment of the “interferon alpha response” pathway in THP1-NLRC4 (T337S) cells versus WT NLRC4 (**Suppl. Figure 11C**). Lastly, treatment of human primary monocytes with Needle (at 0.1 ng/ml) used to activate endogenous NLRC4 was able to recapitulate the upregulation of the top Type-I IFN genes observed in the NLRC4 expressing cell lines (including *IFI44*, *IFI44L*, *CXCL10*, *IFIT3*) and after NLRC4 (T337S) mRNA transfection in human primary monocytes (**Suppl. Figure 12**). Importantly, in this condition we were not able to detect any significant increase of inflammasome activation readouts (caspase-1 activity and IL-18 secretion). As positive control, robust inflammasome activation could be detected at higher Needle concentration (1 ng/ml), although the levels of Type-I IFN genes were not increased compared to lower Needle concentration (0.1 ng/ml). Altogether, the combination of these various cellular models indicates that NLRC4 expression and activation can trigger a Type-I IFN transcriptional program, without robust canonical inflammasome activation.

To confirm and extend this finding in human disease, we observed that *NLRC4* expression (but not *NLRP10* used a control) strongly correlated with expression of the Type-I IFN genes induced in the NLRC4-expressing cell lines (as described in Figure 3C) in various patient cancer samples (colon, lung, and melanoma) (**Figure 4A**). To further validate this, we found that *NLRC4* expression (but not *NLRP6* used as control) was also correlated with a broader unbiased Type-I IFN gene signature (encompassing 59 genes, see methods) in colon COAD

and READ patient tumors ( $R=0.46$ ,  $p<2.2e-16$ ;  $R=0.53$ ,  $p=5.2e-14$ , respectively), as well as in lung LUSC and LUAD patient tumors (**Figure 4B**). We extended the same analysis to other NLR-family members and observed that *NLRC4* expression shows the highest correlation with the Type-I IFN signature overall across most tumor types ( $R>0.5$ ), whereas most of the other NLRs show low to no correlation (**Suppl. Figure 13**). Importantly, consistent with our finding showing the role for *NLRC4* in protecting against metastatic progression in CRC, expression of *NLRC4* (but not *NLRP10*) and Type-I IFN genes were associated with a significantly lower risk of metastasis in skin cutaneous melanoma (SKCM) patients (**Figure 4C**). In human colorectal cancer, mismatch repair-deficient (MMRD) patient tumors have been shown to have better antitumor immunity with cytotoxic T cell infiltration and response to immune checkpoint blockade (12). An enriched immune hub within mismatch repair-deficient tumors has been identified, composed of activated T cells and malignant cells expressing IFN-stimulating genes (ISGs) and CXCR3 ligands (12). Since our results demonstrate that *NLRC4* expression in colon cancer cells mediates Type-IFN signaling and is associated with T cell infiltration and better prognosis in patients, we hypothesized that *NLRC4* expression might be associated to microsatellite instability (MSI) in patient tumors. To test this hypothesis, we utilized the TCGA dataset and observed that *NLRC4* expression was significantly higher in MSI High versus Low COAD tumors, in contrast to other NLR-family members including *NLRP6* and *NLRP10* (**Figure 4D**). By extension, we confirmed that *IFI44L* expression (top Type-I IFN gene upregulated in *NLRC4*-expressing cell lines) was significantly higher in MSI<sup>high</sup> tumors along with the larger gene set encompassing the top 14 Type-I IFN genes upregulated in *NLRC4*-expressing cell lines (**Figure 4E**). Hence, *NLRC4* expression can trigger a Type-I IFN immune reprogramming in human cancer cells that is observed in patient tumors from various cancer types and confers lower risk of metastatic progression.

## ***NLRC4* expression is associated to DC and CD4<sup>+</sup>/CD8<sup>+</sup> T cell immune infiltration in patient tumors**

Type-I IFN signaling is critical in priming professional antigen-presenting cells (APCs), including DCs, for tumor antigen presentation and co-stimulation of T cells. It also provides the cues for Th1 polarization and T cell licensing for tumor cell killing (13). Analysis of the multiple human DC subsets (14) showed the strongest correlations of *NLRC4* expression with DC2, DC3, and DC4 subsets in COAD (R=0.69, 0.71, and 0.64 respectively) as well as in READ patients. Those same three subsets were also the most correlated ones in lung cancer (LUSC: R=0.81, 0.78, and 0.81 respectively; similar magnitude for LUAD) as well as in melanoma SKCM (**Figure 5A, left**). Strikingly, the same analysis performed with *STING/TMEM173* expression (well characterized Type-I IFN signaling mediator) provided much lower coefficient correlations than *NLRC4* for those DC2/DC3/DC4 subsets in both colon and melanoma patient tumors, indicating the role of *NLRC4* expression as a critical driver of DC tumor infiltration in multiple cancer types. Correlation analysis between infiltration of DC2 or DC3 subsets and *NLRC4* expression in COAD patient tumors showed robust associations for either of these cell subsets (R=0.73,  $p < 2.2 \times 10^{-16}$ ; R=0.72,  $p < 2.2 \times 10^{-16}$  for DC2 and DC3 respectively), in comparison to *NLRP10* and *TMEM173* (**Figure 5A, right**). An extended analysis of additional Type-I IFN inducers showed that *NLRC4* expression has the highest correlation overall across the various DC subsets and tumor types, followed by *IFIH1*, *RIGI*, *TMEM173*, and finally *ADAR* (**Suppl. Figure 14**). To further evaluate the robustness of these results, we leveraged multiple DC signatures from immune cell de-convolutional tools where signatures were derived from bulk RNA-seq analysis of sorted cells. Overall, we obtained higher correlations of those DC signatures with *NLRC4* compared to *TMEM173* expression in colorectal and lung cancers (**Suppl. Table 2**). Noteworthy, the molecular features of DC2 and DC3 subsets by scRNAseq analysis have suggested an inflammatory monocyte phenotype and

Type-I IFN signaling/Antigen presentation functions (14). Aligned with those molecular features, DC2/DC3 subsets mediate CD4<sup>+</sup> and CD8<sup>+</sup> T cell proliferation (14). Consistent with those observations, *NLRC4* expression (which we found associated to DC2/DC3 subsets in cancer tumors) correlated strongly with *CD4* expression (R=0.69, p<2.2e-16) in COAD patient tumors, and *CD8A* to a lesser extent (R=0.47, p<2.2e-16) (**Figure 5B, left and right**). Similar results were extended for lung and melanoma cancers (**Figure 5B, left**). As a control, neither *NLRP10*, *TMEM73* (**Figure 5B, right**), nor downstream inflammasome cytokines *IL1B* and *IL18* or *CASP1* (**Figure 5C, Suppl. Figure 15 and 16 and Suppl. Table 3**) correlated with *CD4* or *CD8A* expression to the same extent as *NLRC4* expression. Therefore, consistent with its association to Type-I IFN signaling genes observed in our previous analyses, *NLRC4* expression strongly correlates with infiltration of antigen-presenting DC phenotypes and CD4<sup>+</sup>/CD8<sup>+</sup> T cells in colon and lung patient tumors.

**NLRC4 expression in human cancer cells mediates the release of Type-I IFN chemokines and myeloid growth factors to directly mature DCs *in vitro*.**

Based on the results obtained from patient tumors and the fact that HT29-NLRC4 human cancer cells are reprogrammed towards Type-I IFN signaling, we hypothesized that key immune mediators and growth factors could be released from these cells to mediate T cell/DC infiltration and differentiation. We observed first a robust release of Type-IFN chemokines CXCL10 and CCL20 (to a lesser extent) from HT29-NLRC4 cells versus mock control Pex cells, along with myeloid growth factors M-CSF and GM-CSF, independently of exogenously added IFN $\gamma$  (**Figure 6A, left**). As a control, we confirmed the absence of inflammasome-dependent IL-1 $\beta$  and IL-18 release in response to NLRC4 expression and/or IFN $\gamma$  treatment. Consistent with our observation, CXCL10 was shown to direct the polarization of CD4<sup>+</sup> T cells into potent effector IFN $\gamma$ <sup>high</sup> IL4<sup>low</sup> Th1 cells (15), and low transcript levels of *CXCL10* in colorectal cancer

patients are associated with poor prognosis (16). CCL20 is involved in DC homing to gut-associated lymphoid tissue (17). Next, a broader untargeted secretomics analysis revealed additional Type-I IFN chemokines being released by NLRC4-expressing cells such as CXCL1, CXCL6, CXCL9, inflammatory cytokines (TNF, LIF, IL-8), and growth factors involved in immune cell proliferation (TGF-beta-1, FGF-19, SCF, VEGFA, TGF-alpha) (**Figure 6A, right**). To explore the capability of tumor-cell-derived NLRC4 expression to mediate direct DC maturation for T cell activation, we co-cultured HT29-NLRC4 cells with freshly isolated human primary DCs from human blood. Co-cultures between HT29-NLRC4 cells with DCs induced a significantly higher release of IL-12 compared to pEx control cells in the presence of LPS priming (while being maintained at same background level with cultures alone of HT29-NLRC4 cells, pEx control cells, or DCs; in the presence or not of LPS) (**Figure 6B, left**). These results were confirmed at various LPS concentrations (**Figure 6B, right**). We also identified IFN $\gamma$  and IL-1 $\beta$  as following the same pattern as IL-12 (**Figure 6C**), in contrast to IL-2 and IL-10, used as a control (**Suppl. Figure 17A**). Broader untargeted proteomics analysis on these co-cultures also identified the Th1 polarizing cytokine IL-18 and additional mediators involved in DC proliferation/differentiation (STAMBP, Flt3L, 4E-BP1) being significantly released by DCs in the presence of NLRC4 expressing cells (**Figure 6D**). The plotted curves of the additional analytes captured by untargeted secretomics are shown in **Suppl. Figure 17B**. Consistently, the combination of these multiple NLRC4-induced mediators secreted by DCs (GM-CSF, IFN $\gamma$ , Flt3L) has been shown to robustly mature DCs for IL-12 production and Th1 stimulation (18). Since DC-mediated IL-12 and IL-18 secretion is critical in mediating T/NK cell cytotoxicity and Th1 polarization, including licensing cytotoxic CD8 $^+$  T cells in their antitumor activities (19, 20), we established here that altogether NLRC4 expression in human cancer cells is sufficient to directly mediate the release of critical cytokines and immune mediators to drive DC maturation towards Th1 polarization *in vitro*. Hence, these mechanisms

contribute to explain the association between NLRC4 expression and DC/T cell tumor immune infiltration we observed in patient tumors, which correlates with improved survival.

**LPS specifically down-regulates *NLRC4* expression but no other NLR-family members in human primary cells.**

Progression to colon metastasis in patients has been suggested to be linked to the presence of higher LPS in mucosal tissues (21). To test whether LPS treatment affected expression of *NLRC4* in human immune cells, we stimulated primary monocytes and macrophages *in vitro* and found that *NLRC4* gene expression, along with its adaptor *NAIP* required for pathogen sensing, were dramatically reduced by LPS treatment in these cells (**Suppl. Figure 18A**). Strikingly, such decrease was not observed for other NLR-family members *NLRP3* and *NLRP1* (**Suppl. Figure 18B**), nor for the inflammasome gene *CASP1* (**Suppl. Figure 18C**). The transcription factor IRF8 (which can control *NAIP* and *NLRC4* gene expression in mice) (22) was rather increased by LPS treatment (**Suppl. Figure 18C**), thereby suggesting another mechanism of repression independent of IRF8. Therefore, the presence of LPS-expressing bacteria may provide a mechanistic link between the loss of NLRC4 protein expression in CRC patient tissues and metastatic progression. Indeed, increasing evidence suggests that bacterial infection not only promotes carcinogenesis but also affects metastatic progression and organ selectivity through modification of the microenvironment at primary and secondary tumor sites (as reviewed in (23)).

## **DISCUSSION**

Here we describe a novel role for epithelial NLRC4 in cancer progression and invasiveness. Its expression in cancer cells predicts patient survival and modulates anti-tumoral immune responses in humans. We identified that tumor epithelial expression of NLRC4, rather than

stromal, is critical to mediate immune protection through DC and CD4<sup>+</sup>/CD8<sup>+</sup> T cell immune infiltration into the tumor microenvironment. Mechanistically, we show that epithelial human NLRC4 expression can engage an immune transcriptional program combining Type-I IFN gene signaling and chemokine production, enabling the direct maturation of DCs towards a Th1 antitumor immune response *in vitro*. This underlying mechanism may explain our observed strong associations between NLRC4 tumor expression with DC2/DC3 and CD4<sup>+</sup>/CD8<sup>+</sup> T cell infiltration into patient tumors for antigen presentation and tumor killing, respectively. Therefore, epithelial NLRC4 expression is signaling critical information between the epithelial innate and adaptive immune responses against metastatic cancer progression leading to improved patient survival.

The decreased protein expression of NLRC4 in the tumor bulk and its correlation to poor prognosis in CRC patients is consistent with a previous report (24). To note, upregulation in astrocytes was associated to poor prognosis in glioma patients (25). Our results show that in contrast to epithelial-expressed NLRC4, loss of IL-1 $\beta$  expression is not associated with disease prognosis. Hence, the impact of NLRC4 expression on the prognosis of CRC and protection against metastatic progression is unlikely to be mediated by downstream inflammasome pathway components alone. In comparison to mouse models, our results in patients are consistent with a previous study showing *Nlrc4*<sup>-/-</sup> mice displayed increased colon tumorigenesis in the AOM/DSS model wherein tumors appeared aggressive with invasion of tumor cells below the muscular mucosae (10). Another study using AOM/DSS showed no difference in *Nlrc4*<sup>-/-</sup> mice (26). To note, a pro-tumorigenic role of NLRC4 coming from the myeloid compartment has been described in mouse models of high fat diet-induced colorectal and breast cancers (27, 28), although the tumor-intrinsic role of NLRC4 has not been investigated. NLRC4 is normally constitutively expressed in human intestinal epithelial cells (IECs) along with proIL-18 (29), to cope with extracellular insults by sensing through NAIP the presence of

infection and microbiome dysbiosis directly, thereby participating in maintaining the gut barrier integrity. However, when rendered hyperactivated by mendelian gain-of-function mutations, NLRC4 induces a spectrum of clinical autoinflammatory syndromes characterized by severe enterocolitis and gut inflammation (5–7). These clinical features are clearly different than in NLRP3 GOF-inducing CAPS diseases (cryopyrin-associated periodic syndrome). This observation suggests that activated NLRC4 triggers non-redundant immune mechanisms in the gut compared to other NLRs.

At the molecular level, we have identified novel functions for human NLRC4 in triggering an immune cellular reprogramming with Type I-IFN signaling and the production of a broad array of signaling molecules *in vitro* (chemokines, inflammatory cytokines and growth factors) involved in the chemotaxis, proliferation, and activation of immune cells. In our study, expression of Type-I IFN genes by human NLRC4 can occur in the absence or presence of robust inflammasome activation. Therefore, both NLRC4 functions do not seem to be mutually exclusive but may act in concert if needed. Since Type-I IFNs also induce *IL18* gene expression (29) and IL-18 upregulates MHCII expression in epithelial intestinal cells (30), we speculate that epithelial-intrinsic NLRC4 inflammasome activation may enhance local T cell activation through both Type-I IFN signaling and mature IL-18 production.

Consistent with our results in humans, a Type-I IFN signaling pathway was identified among the top upregulated gene networks in a patient harboring a dominant activating mutation in *NLRC4* (T337S), which leads to Macrophage Activation Syndrome (MAS) (5). Also consistent with our correlation of T cell infiltration in cancer patients with NLRC4 protein expression, an increase of gut intra-epithelial lymphocytes was detected in the patient harboring the *NLRC4* activating mutation V341A leading to enterocolitis autoinflammatory syndrome (6).

Important molecules mediated by human NLRC4 expression identified here include the CXCL10 chemokine and other family members, which are critically involved in the T cell-

mediated antitumor immune response (15, 16, 31–34). We show that NLRC4 expression in human tumor cells is sufficient to directly promote DC maturation to secrete IL-12 and IFN $\gamma$  *in vitro*, along with the inflammatory cytokine IL-1 $\beta$ . DC-mediated IL-12 secretion is key in mediating T/NK cell cytotoxicity and Th1 polarization, including licensing cytotoxic CD8<sup>+</sup> T cells in their antitumor activities in the context of anti-PD1 immunotherapy (19, 20). Our findings indicate that this cytokine may, at least in part, mediate the downstream effects of NLRC4 expression in modulating the antitumor immune response against human colorectal cancer and possibly other epithelial cancers. Our results support a mechanism by which *NLRC4* expression drives DCs (mainly DC2/DC3/DC4 subsets) and CD4<sup>+</sup>/CD8<sup>+</sup> T cell infiltration into patient tumors. DC2 and DC3 subsets express molecular features of antigen presentation as shown previously by scRNAseq and promote CD4<sup>+</sup>/CD8<sup>+</sup> T cell activation/proliferation in co-cultures (14). In human colorectal cancer, high MSI patients with mismatch repair-deficient (MMRD) tumors have been shown to have better antitumor immunity with cytotoxic T cell infiltration and response to immune checkpoint blockade (12). An enriched immune hub within mismatch repair-deficient tumors has been identified composed of activated T cells and malignant cells expressing IFN-stimulating genes (ISGs) and CXCR3 ligands. We show here that higher *NLRC4* expression is also associated with MSI high colorectal patient tumors. Putting these results into context with our observations, we can further refine this model and propose a critical role for epithelial-expressed human NLRC4 to trigger DC2/DC3 and T cell infiltration through Type-I IFN signaling and chemokine production to subsequently prime and activate T cells for tumor killing. As a result, NLRC4 expressed in the epithelium prevents progression to a more aggressive metastatic stage of CRC by contributing to this antitumor immune hub. Additionally, since MSI high status predicts better responses to immune checkpoint blockade (ICB) immunotherapies and NLRC4 associates with improved T cell infiltration conferring better prognosis, we hypothesize that NLRC4 expression might provide

a better response to ICB or broaden the scope of potential patient responders. Our observation that *NLRC4* expression is strongly associated mainly with CD4<sup>+</sup> T cell infiltration and *CD4* gene expression more potently than *CD8A* in patient tumors indicates that NLRC4 might play a predominant role in the acquisition of CD4<sup>+</sup> T cell cytotoxic function, previously demonstrated to be critical for mounting a productive antitumor immune response (35). This effect could be explained by the infiltration and maturation of tumor-antigen presenting DC2 cells, as observed in melanoma patients (36).

The identity of DAMPs or PAMPs which activate human NLRC4 in epithelial tumor cells leading to the phenotypes described in this study warrants further investigation. In addition to its role in sensing bacterial pathogens, NLRC4 activation can be triggered by sterile DAMPs produced during metabolic dysregulation or expression of endogenous retrotransposons (3, 4). Since SINE RNAs robustly accumulate early during malignant cellular transformation (37) and de novo purine synthesis contributes to the proliferation of cancer cells (38), we speculate that these DAMPs could be sensed intrinsically by epithelial-derived NLRC4 leading to a robust immune response. Finally, we show that the loss of NLRC4 expression in patient tumor tissues may be due to the presence of LPS (expressed by gram-negative bacteria) which specifically abolished *NLRC4* expression at the transcriptional level but no other NLR-family members in human primary cells. These results are consistent with previous findings demonstrating that LPS promotes metastatic progression in colorectal cancer through a NF- $\kappa$ B/Snail/HK3 signaling axis that potentiates glycolysis and increases migration and invasion (21). Therefore, the loss of *NLRC4* transcript might be mediated through this axis (since *IRF8* remains unchanged) and be explained by the presence of LPS-enriched microbiome present in patients. In summary, we propose a novel mechanism of immune protection against tumors in humans mediated by the expression of epithelial NLRC4. Our combined analysis using genetic editing, RNA sequencing and proteomics enabled us to identify the pathway by which NLRC4

expression associates to enhanced DC profiles and T cell responses in cancer patients, controlling the evolution of the disease and improving the survival of patients. This work sheds light on epithelial NLRC4 in providing critical priming signals to improve DC/T cell immune response in humans, thereby eventually sensitizing the tumor to current T cell centric ICB therapies. These results might lay the foundation for novel therapeutic opportunities in CRC and other epithelial cancer types by extension including lung and skin melanoma.

## **MATERIALS AND METHODS**

**Sex as a biological variant:** both sexes were involved, and sex was not considered as a biological variable.

**Tissue micro-arrays (TMAs) from the Bergonié Cancer Institute:** 104 patients treated for primary CRC at the Bergonié Institute (Bordeaux, France) between May 2008 and January 2013 were enrolled. Histology samples were obtained from surgery, and tissues were fixed in formalin and then paraffin embedded (FFPE). Clinical characteristics were collected from patient medical charts with special focus on age, gender, date of diagnosis and tumor node metastasis (TNM) stage. Histological type was determined as well as tumor grade, and mutational status. Tissue cores with a diameter of 0.6 mm were removed from FFPE blocks and arrayed on a recipient paraffin block using a tissue arrayer (Beecher Instruments Tissue Arrayer, Sun Prairie, WI) at the Molecular Biology Department of Bergonié Institute. Each tumor sample was punched in triplicate, along with 2 cores of matched normal mucosal tissue punched far away from the tumor. Sections of the array were cut at 5  $\mu$ m and placed on glass slides.

**Tissue micro-arrays from the commercial USBiomax cohort:** In the CO2161 TMA (USBiomax Inc.; Rockville, MD), there were 204 colon adenocarcinoma, 4 signet-ring cell

carcinoma and 8 unmatched normal colon tissues, with one core for each tumor case. Adenocarcinoma were from pathologic stage I (n=22), stage II (n=128), stage III (n=47) and stage IV (n=11) (Suppl. Table 1). Slides were treated similarly as the Bergonié's TMA slides, and were stained only with NLRC4, and cytokeratin (see in the corresponding section).

**Immunofluorescence tissue staining:** Immunofluorescent analysis was performed on a 5- $\mu$ m fixed paraffin-embedded TMA section mounted on a charged slide. Tissues were deparaffinised in xylene and rehydrated in a series of ethanol baths. Heat-induced proteolytic epitope retrieval was done in target retrieval buffer (DAKO pH 6.0 #S236984 or pH 9.0 #S236784, Agilent) according to primary antibody using a microwave oven for 20 minutes. Slides were then blocked using 5% BSA for 10 minutes. Primary antibodies (see below) were incubated in antibody diluent (DAKO, #S202230, Agilent). Secondary antibodies [goat anti-rabbit (Alexa Fluor 594 nm), goat anti-mouse (AF 488 nm) and donkey anti-goat (AF594 nm), ThermoFisher] were diluted (1/400) in antibody diluent. Sections were washed with PBS and incubated with DAPI (2  $\mu$ g/mL) for 10 minutes. Finally, slides were mounted with Fluoromount-G and stored at 4°C. NLRC4 (Abcam; #AB115537), Caspase-1 (p10) (LS Bio; #LS-C312683), IL-1 $\beta$  (Cell Signaling; #3A6), IL-18 (Sigma; #HPA003980); pan-Cytokeratin to stain specifically epithelial cells (AE1-AE3 clone). Before use on TMA slides, we assessed antibodies' specificity by western-blot or immunofluorescence assay on cell lines fixed in formalin and paraffin-embedded.

### **Image acquisition from TMA**

*Image handling:* Images of the TMA are generated using the slide scanner NanoZoomer from Hamamatsu. Homemade software was designed to perform the processing adapted to the study.

*Cytokeratin detection:* Epithelium is detected using a simple threshold intensity on the cytokeratin channel followed by a morphological closing operation to fill up small holes in the segmented region. The obtained region can be used to distinguish Epithelium structure from the rest on the image. It also can be transferred to a consecutive slice to reveal the position of the Epithelium in the consecutive slides.

*Cell detection:* Nuclei DAPI channel is used to drive cell segmentation. Nuclei are detected using band-pass followed by thresholding above the background. Nuclei clusters are splitted using watershed strategy to obtain well separated nuclei segmentation. Cell segmentation is obtained by defining rings around nuclei. Rings of fixed width define the cytosolic area around nuclei.

*Feature measurements:* For each cell, intensity features are measured from fluorescent channels using maximum or median or average operators. Measurements are extracted for the different subcellular compartments (cells, nuclei and cytosol). Cell statistics are stored into “csv” files for further analysis.

*Core alignment:* To perform correlative analysis between the different channels, a method based on image registration was developed and used. For each core, image registration based on the DAPI channel was applied. DAPI channel is used because it is the channel which is the most conserved from one slide to another. The image registration consists in finding the best rigid transform (translation + rotation) that allows to fit the first image into the second. This best transform is applied to all channels of the first slide. A new multiplexed image is obtained combining all channels of the first slice and all channels of the second slide. This multiplexed image is used to apply Cytokeratin mask detection to consecutive images.

*Cytokeratin region transfer:* To be able to transfer the epithelium region to a consecutive slide, nuclei channel of a core image is registered to nuclei channel in the consecutive slide. Nuclei repartition and density contains enough information to estimate the rotation and translation need

to register the first image on the second one. The estimated rotation and translation are applied to the full core image and the epithelium region mask. Epithelial region mask is now precisely aligned to the consecutive slice.

*Cytokeratin mask detection:* The cytokeatin mask is obtained by processing cytokeatin channel using direct thresholding followed by morph math operations (opening and closing). This mask is used as a channel such as a feature to express whether the cell is in or out the cytokeatin mask.

*Cell positivity:* Cell positivity is obtained by placing one or several thresholds on selected features. For example, we have counted the number of cells that are positive for a certain biomarker and inside the cytokeatin mask. The positive cells were displayed on the screen such as the user can control and finetune the threshold. After staining, slides were then digitalized with the Hamamatsu Nanozoomer 2.0HT scanner in collaboration with the Bordeaux Imaging Center (BIC). Imaging acquisition and fluorescence quantification was made by QuantaCell Inc. (Montpellier, France).

After computer-assisted image calibration, immunofluorescence quantification was obtained by measuring the fluorescence of each pixel in a DAPI-positive cell, calculating the median of all pixels in each cell and then assessing the mean of median intensity of all cells for each spot. Studied cells were identified with DAPI staining and epithelial cells (in normal and tumor tissues) with a cytokeatin mask (Supplemental Figure 1). Indeed, quantification of inflammasome expression was done by applying a cytokeatin mask on each spot, to measure fluorescence of inflammasome markers only in cytokeatin/epithelial positive cells. Images were reviewed with NDP.View 2 (Hamamatsu photonics Inc).

**Immunohistochemistry:** Immunohistochemical analysis was performed in all cases on 3  $\mu\text{m}$ -thick serial sections from a representative formalin-fixed, paraffin-embedded (FFPE) block. We used the following antibodies: CD3 (clone 2GV6, prediluted, Roche Diagnostics), CD8 (clone C8/144B, dilution 1/25, Dako Glostrup, Denmark), CD68 (clone PG-M1, dilution 1/50, Dako Glostrup, Denmark), CD163 (clone 10D6, dilution 1/100, Leica Novocastra Laboratories, United Kingdom). In 32 cases, heterologous differentiation was suspected and additional antibodies against desmin (clone D33, dilution 1: 100, Dako, Glostrup, Denmark), h-caldesmon (clone h-CD, dilution 1: 50, Dako), and myogenin (clone LO26, dilution 1: 20, Novocastra, New Castle upon Tyne, United Kingdom) were used. After microwave oven heating (20 min in 0.1 M citrate buffer at pH 6), sections were incubated with biotinylated link antibody, with peroxidase-labelled streptavidin (LSAB<sup>TM</sup> + Kit; Dako) and then with diaminobenzidine solution (DAB; Dako). Omitting the specific primary antibody was used as negative controls. Levels of tumor infiltration by immune cells was assessed by an expert pathologist based on cell morphology and organization. Then, levels of tumor infiltration specifically by CD3<sup>+</sup> and CD8<sup>+</sup> cells (T cells), or CD68<sup>+</sup> and CD163<sup>+</sup> cells (macrophages) were assessed as Low, Moderate, or High.

**Cloning procedure and control:** cDNA encoding *NLRC4* was amplified by RT-PCR and directly ligated into a lentiviral vector. The cherry vector was provided by Genecopoeia (#pEX-T3678-Lv130) and *NLRC4* was already ligated in the vector. In this vector, *NLRC4* is fused in C-terminal with a red fluorescent protein cherry. Lentiviral particles were produced by transient transfection of packaging 293T HEK cells and viral titers were determined by enzyme-linked immunosorbent assay of p24. Transductions of HT29 were performed using lentiviral particles produced by transient transfection of 293T HEK cells. Different MOI were used in RPMI 1640 medium with 8% of fetal bovine serum and glutamine. Purity was assessed by FACS and cells

from correct MOI were sorted by flow cytometry (BD FACSAria). *NLRC4* expression was assessed by RT-qPCR and western-blot (primary antibody Abcam; #AB115537 dilution of 1/1000°; fluorescent secondary antibody dilution 1/4000° IRDye®).

**Proliferation assay:** Cell division was assessed using carboxyfluorescein diacetate succinimidyl ester (CFSE) dye (Life Technologies®, #V12883). Transduced cells with NLRC4-cherry or mock-cherry were trypsinized, spin down and resuspended at 10<sup>6</sup> cells/ml in PBS containing CFSE at a final concentration of 1.5 µM. Cells were stained during 10 mn at 37°C and then washed in hot sterile PBS. Cells were centrifuged and resuspended in complete medium at a concentration of 10<sup>6</sup> cells/ml during 30 mn at 37°C. Cells were then washed twice in medium and 20 000 cells/well were seeded in 24-wells. Cell division was analyzed every 24 hours detecting fluorescence by flow cytometry, until 7 days.

**Scratch wound healing assay:** Cells were seeded at 400 000 (HT29) or 450 000 (SW620) cells/well in a 24-well culture plate. Cells were cultured until being 80% confluent as a monolayer. After 24 hours of growth, a 200 µl pipette tip was used to form a wound. Each well was gently washed twice with medium to remove detached cells, and cells were cultured for further 24 h. A x4 microscope was used to take pictures and the scratch surface was assessed at each time point using ImageJ software.

**Differential gene expression by RNAseq analysis:** RNA-Seq sample analysis was performed using Array Studio software version 10.0.1.81 (QIAGEN®, Cary, NC), the OSA aligner, and the OmicsoftGene20130723 gene model (39). Aligned count matrixes were used as input into a DESeq2 workflow to measure differential gene expression (40). Genes with an absolute log fold change of greater than 2 and an adjusted Pvalue of less than 0.05 between two conditions

were considered as significant. Significant genes were used as input to the pathfinder R package to measure altered KEGG pathways (41, 42).

**Bioinformatic analysis from public datasets: profiling of immune cell infiltrates, survival, correlation of gene expression:** Immune cell type gene signatures were from CIBERSORT (43). DC subset gene signatures were from scRNA-seq study of human blood DC (14); TCIA (44); TIMER (45). Type I IFN regulated genes were those reported on the QIAGEN Human Type I Interferon Response PCR Array and whose upregulation by type I IFN were confirmed by at least two studies in Interferome database. Pearson correlation analysis was performed for each pair of gene vs. immune cell type, gene vs. gene for their expressions in COAD (colon adenocarcinoma), READ (rectum adenocarcinoma), SKCM (Skin cutaneous melanoma), LUSC (lung squamous cell carcinoma) and LUAD (lung adenocarcinoma) from TCGA transcriptomic data. The expression value of cell type signature was represented by the median value of genes in the specific gene set. TIMER analysis (45) was conducted on the corresponding website. ggpubr and ggplot2 package in R were used for statistical calculations and visualization. Comparisons of NLRC4 between tumor samples vs. related normal were conducted in “TCGA land” by OmicSoft. Survival analysis was performed in ClinicalOutcome dataset compiled by OmicSoft([http://www.arrayserver.com/wiki/index.php?title=Introduction\\_to\\_ClinicalOutcome\\_Land\\_Content](http://www.arrayserver.com/wiki/index.php?title=Introduction_to_ClinicalOutcome_Land_Content)). ClinicalOutcome contains human gene expression profiles associated with key clinical features and outcomes like “Survival”, etc. from GEO.

### **Intestinal APC<sup>-/-</sup> in vivo mouse model**

*Mice:* *Apc*<sup>Min/+</sup> mice were obtained from The Jackson Laboratory and bred in house and experiments were performed according to the guidelines of the animal ethics committee of

McGill University (Canada). Mice were sacrificed at 3 or 6 months of age. Small intestine and colon were removed from animals, flushed with cold PBS supplemented with penicillin and streptomycin, and cut longitudinally for polyp enumeration.

*Hematoxylin and Eosin (H&E) staining and immunofluorescence:* Small intestines were fixed and paraffin-embedded subsequently. H&E sections were scanned using ScanScope XT digital scanner (Aperio Technologies). For immunofluorescence, slides were de-paraffinized by washing in xylene. Antigen retrieval was performed, and slides were permeabilized with 0.25% Triton X-100 in PBS and washed in PBS 0.05% Tween 20. Slides were then blocked (10% FBS, 3% BSA (Bioshop, #ALB001)) for 30 minutes at 37°C and tissues were incubated with primary antibodies in PBS containing 3% BSA, overnight at room temperature. Primary and secondary antibodies were diluted in 3% BSA PBS. Primary antibodies used include Nlrc4 (Novus #NBP1-78980) and Cytokeratin (AE1/AE3) (Dako # M3515). Tissues were mounted with cover slips and analyzed on a Zeiss Axioskop upright wide-field microscope (20x/0.5 or 40x/0.75 Plan-Neofluar objectives) equipped with a high-resolution monochromatic AxioCam HRm camera and driven by AxioVision version 4.9.1 (Carl Zeiss Microscopy). ImageJ 1.46 (National Institute of Health) was used for processing of entire images before cropping to emphasize the main point of the image when appropriate; processing was limited to background subtraction, brightness/contrast adjustments and pseudo colors addition to facilitate the visualization/interpretation of the results.

**mRNA transfection of human primary monocytes:** Polyadenylated CleanCap<sup>®</sup> In vitro transcribed (IVT) mRNA fully substituted with 5-methoxyuridine encoding EGFP, NLRC4 (V341A) or NLRP3 (R260W) was purchased as a custom order from Trilink biotechnologies. 9 pmoles of each IVT mRNA was electroporated into peripheral primary human monocytes

using the 4D-Nucleofector System™ (Lonza) with the P3 Primary Cell 4D-Nucleofector™ X Kit L (program EA-100). 24 hrs following electroporation, supernatants were harvested and assayed for caspase-1 activity using Caspase-1-glo® (Promega) and IL18 levels were measured using the MSD® Multi-Spot assay system. Total RNA was isolated from the cellular fraction of triplicate-pooled samples using the RNeasy kit (Qiagen cat 74106) and subjected to cDNA synthesis using the Iscript cDNA synthesis kit (Biorad cat 1708891). Quantitative PCR was performed on cDNA samples using Taqman primer/probes purchased from ThermoFisher Scientific. Data are normalized to the levels of the housekeeping gene (ACTB) and plotted as fold change control transfection.

**Co-cultures of human primary DCs and maturation, and secretomics analysis:** HT29 colorectal cancer cells containing either pEX (ref. #pEX-T3678-Lv130) empty vector or pEX-NLRC4 were cultured according to previously stated conditions (Gibco RPMI 1640, 8% FBS, 200 mM Glutamine - Glutamax cat. #35050061). HT29 cells were grown to 60-70% confluency then trypsinized (Gibco cat. #25300120) and counted using Trypan Blue 0.4% VWR (cat. #K940) for dead cell exclusion. HT29 pEX and HT29-NLRC4 cells were plated on 96-well plates (VWR cat. #10861-562) at 35,000 cells per well. Buffy Coats from healthy donors at the Stanford Blood Center were collected and PBMC were isolated using density-gradient centrifugation (Ficoll-Paque - GE Healthcare cat. #17-1440-02) and enriched for dendritic cells with STEMCELL technologies EasySep Human Pan-DC Pre-enrichment kit (cat. #19251, EasySep magnet cat. #18000/EasyEights cat. #18103, EasySep buffer cat. #20144). DCs were counted and plated at a 1:1.2 ratio (35,000 HT29 : 43,000 DC) on top of HT29s in pre-plated 96-well plates. Lipopolysaccharide (LPS) (Invitrogen cat. #00-4976-93) was added to co-cultures at 0, 0.1, 0.316, 1, 2, 3.16, 10, 31.62 µg/mL concentrations in either duplicates or triplicates. Co-cultures continued for 24 hrs and cell supernatants were centrifuged, placed in

fresh tubes, and frozen at -20°C. Quantikine IL-12 p70 ELISA (R&D Systems cat. # D1200) was performed according to manufacturer directions to assess DC priming. In parallel, same cell supernatants were submitted to secretomics analysis using Olink Proteomics. Samples were prepared for and analyzed using the multiplex Inflammation I according to manufacturer's instructions (Olink Biosciences, Uppsala, Sweden). To calculate the differential protein expression, a linear model was fitted with the log<sub>2</sub> normalized protein expression levels as the dependent variable. For these calculations, we only used LPS-induced samples. P-values were adjusted by multiple testing using Benjamini-Hochberg method (46).

**Cellular models of NLRC4 (T337S) mutant expression:** Primary human monocyte-derived macrophages and NLRC4-transduced THP1 cells were generated as in (5). Briefly, primary macrophages were generated from CD14-selected peripheral blood monocytes by culturing in M-CSF for seven days. Stably transduced THP1 cells were stimulated with 10ng/mL PMA for up to 72 hours. Cells were lysed in Trizol, RNA isolated, and RNA integrity analyzed with the Agilent 2200 TapeStation. Messenger RNA purification and fragmentation, cDNA synthesis and target amplification were performed with Illumina TruSeq RNA Sample Preparation kit. Pooled cDNA libraries were sequenced on Illumina HiSeq 2500, mapped to XXXX, gene track XXXX, quantified using CLC Main Workbench software (V22, Qiagen), and expressed as TPM. Heatmaps were generated using Morpheus (<https://software.broadinstitute.org/morpheus>). Gene Set Enrichment Analysis (GSEA) was performed on untrimmed TPM comparing T337S mutant- vs WT-transduced THP1 cells at 24 hours using GSEA v4.1 with the following parameters: permutations=1000; permutation type=gene\_set, Enrichment statistic=weighted, and Ranking metric=Signal2Noise.

**Monocyte or Monocyte-derived Macrophage differentiation and stimulation:** Pan human monocytes were isolated from peripheral blood using column-based isolation according to the manufacturer's protocol (Miltenyi cat 130-021-221). Isolated cells were then cultured in X-Vivo 15 media supplemented with 10ng/mL MCSF (R&D cat 216-MCC-010) for 5 days, prior to stimulating them or freshly thawed monocytes from the same donor with 1ug/mL LPS (Invivogen cat tlrl-pek1ps) for 4 hrs. RNA was then isolated and QPCR performed from cells according to the procedures described above. In experiments with needle-tox, isolated monocytes were rested overnight in media and stimulated the next day with either 0.1ng/mL or 1ng/mL needle-tox (Bacillus thailandensis T3SS needle protein (Needle) mixed with Protective Antigen (ListLabs) at a ratio of 1:8) for the indicated periods of time. Cell supernatants were collected for Caspase-1 activity according to the manufacturers protocol (Promega) or IL-18 secretion was measured by MSD. RNA was then isolated and QPCR performed from cells according to the procedures described above.

**Patient stratification and Statistical analysis:** For patient tissue analysis of expression, clinical and biological measurements were expressed as mean (standard deviation) or median (range) for continuous variables, or as a number (percent) for categorical variables. The comparison between quantitative and qualitative variables was done using a 2-tailed Student t-test (parametric) or the Mann-Whitney U-test (non-parametric). The comparison between qualitative variables was done using a Chi<sup>2</sup> (parametric) or a Fisher's exact test (non-parametric). Variance analysis was done using a one-way ANOVA (parametric) or Kruskal-Wallis (non-parametric) test. A Cox model was applied for survival analysis. Patients were stratified based on high versus low expression of markers according to cut-offs either predetermined by Receiver-Operating Characteristics (ROC) curves (for NLRC4 and IL-18), or by the median of fluorescence intensity (for IL-1 $\beta$ ). A logistic regression analysis was

performed to evaluate the association between NLRC4, IL-18, or IL-1 $\beta$  levels and death within the tumoral tissue and healthy one. ROC curves and area under the curve were computed to assess the impact of marker expression levels for predicting death. Statistical significance was set at  $p < 0.05$ . Data analysis was performed using STATA® software (StataCorpLP, College Station, Texas, USA). ROC curves and threshold determination obtained for NLRC4 and IL-18 are shown in Suppl. Figure 5. However, for IL-1 $\beta$ , sufficient sensitivity and specificity could not be reached to use the determined cut-off and the median of fluorescence intensity was used instead to stratify patients. Others statistical analysis is described in figure legends for other experiments.

**Study approval:** Samples were collected in accordance to french legislation and ethical codes and all patients gave their consents for the use of their biological samples for research purposes.

**Data availability:** RNA-Seq datasets are deposited in Gene Expression Omnibus accession #GSE243588. Supporting data values are provided.

## **AUTHOR CONTRIBUTIONS**

Conceptualization: CD, SC, DF, BF; Methodology: CD, SC, HL, JMB, CC, AN, LL, MFV, ERR, LS, SB, IM, JDC, FL, MD, VV, SN, VP, CR, VR; Investigation: CD, SC, HL, JMB, CC, AN, ERR, LS, SB, LL, MFV, IM, JDC, FL, MD, VV, SN, VP, CP, KN, CR, VR, PB, JDM, MS, SWC, DF, BF; Funding acquisition: PB, JDM, MS, SWC, DF, BF ; Supervision: DF, BF; Writing – review & editing: CD, SC, HL, MS, SWC, DF, BF.

## **ACKNOWLEDGMENTS**

We thank the genomics platform of the University of Bordeaux, and the various research funding agencies: INCa-Cancéropôle GSO, Ligue Nationale contre le Cancer, ARC

Foundation, The MD-PhD program of CHU Bordeaux, CIHR, IDEX Bordeaux, NIH-NIA 1P01AG066591-01A1. We thank Shreya Desikan and Marie-Christin Hoffmann for technical assistance.

## REFERENCES

1. Guo H, Callaway JB, Ting JP-Y. Inflammasomes: mechanism of action, role in disease, and therapeutics. *Nat. Med.* 2015;21(7):677–687.
2. Rauch I et al. NAIP-NLRC4 Inflammasomes Coordinate Intestinal Epithelial Cell Expulsion with Eicosanoid and IL-18 Release via Activation of Caspase-1 and -8. *Immunity* 2017;46(4):649–659.
3. Furman D et al. Expression of specific inflammasome gene modules stratifies older individuals into two extreme clinical and immunological states. *Nat. Med.* 2017;23(2):174–184.
4. Wang S et al. DDX17 is an essential mediator of sterile NLRC4 inflammasome activation by retrotransposon RNAs. *Sci. Immunol.* 2021;6(66):eabi4493.
5. Canna SW et al. An activating NLRC4 inflammasome mutation causes autoinflammation with recurrent macrophage activation syndrome. *Nat. Genet.* 2014;46(10):1140–1146.
6. Romberg N et al. Mutation of NLRC4 causes a syndrome of enterocolitis and autoinflammation. *Nat. Genet.* 2014;46(10):1135–1139.
7. Siahianidou T et al. Autoinflammation with Infantile Enterocolitis Associated with Recurrent Perianal Abscesses. *J. Clin. Immunol.* 2019;39(3):237–240.
8. Romberg N, Vogel TP, Canna SW. NLRC4 inflammasomopathies. *Curr. Opin. Allergy Clin. Immunol.* 2017;17(6):398–404.

9. Kay C, Wang R, Kirkby M, Man SM. Molecular mechanisms activating the NAIP-NLRC4 inflammasome: Implications in infectious disease, autoinflammation, and cancer. *Immunol. Rev.* 2020;297(1):67–82.
10. Hu B et al. Inflammation-induced tumorigenesis in the colon is regulated by caspase-1 and NLRC4. *Proc. Natl. Acad. Sci. U. S. A.* 2010;107(50):21635–21640.
11. Kim H et al. Development of a Validated Interferon Score Using NanoString Technology. *J. Interferon Cytokine Res.* 2018;38(4):171–185.
12. Pelka K et al. Spatially organized multicellular immune hubs in human colorectal cancer. *Cell* 2021;184(18):4734-4752.e20.
13. Demaria O et al. Harnessing innate immunity in cancer therapy. *Nature* 2019;574(7776):45–56.
14. Villani A-C et al. Single-cell RNA-seq reveals new types of human blood dendritic cells, monocytes, and progenitors. *Science* 2017;356(6335). doi:10.1126/science.aah4573
15. Karin N. The Development and Homing of Myeloid-Derived Suppressor Cells: From a Two-Stage Model to a Multistep Narrative. *Front. Immunol.* 2020;11:557586.
16. Jiang Z, Xu Y, Cai S. CXCL10 expression and prognostic significance in stage II and III colorectal cancer. *Mol. Biol. Rep.* 2010;37(6):3029–3036.
17. Sokol CL, Luster AD. The chemokine system in innate immunity. *Cold Spring Harb. Perspect. Biol.* 2015;7(5):a016303.
18. Mosca PJ et al. Multiple signals are required for maturation of human dendritic cells mobilized in vivo with Flt3 ligand. *J. Leukoc. Biol.* 2002;72(3):546–553.

19. Garris CS et al. Successful Anti-PD-1 Cancer Immunotherapy Requires T Cell-Dendritic Cell Crosstalk Involving the Cytokines IFN- $\gamma$  and IL-12. *Immunity* 2018;49(6):1148-1161.e7.
20. Wculek SK et al. Dendritic cells in cancer immunology and immunotherapy. *Nat. Rev. Immunol.* 2020;20(1):7–24.
21. Wu X et al. Lipopolysaccharide promotes metastasis via acceleration of glycolysis by the nuclear factor- $\kappa$ B/snail/hexokinase3 signaling axis in colorectal cancer. *Cancer Metab.* 2021;9(1):23.
22. Karki R et al. IRF8 Regulates Transcription of Naips for NLRC4 Inflammasome Activation. *Cell* 2018;173(4):920-933.e13.
23. Seely KD, Morgan AD, Hagenstein LD, Florey GM, Small JM. Bacterial Involvement in Progression and Metastasis of Colorectal Neoplasia. *Cancers* 2022;14(4):1019.
24. Peng L, et al. Comprehensive Analysis of Prognostic Value and Immune Infiltration of NLRC4 and CASP1 in Colorectal Cancer. *Int J Gen Med.* 2022;15:5425–5440.
25. Lim J, et al. Upregulation of the NLRC4 inflammasome contributes to poor prognosis in glioma patients. *Sci Rep.* 2019;9(1):7895.
26. Allen IC et al. The NLRP3 inflammasome functions as a negative regulator of tumorigenesis during colitis-associated cancer. *J. Exp. Med.* 2010;207(5):1045–1056.
27. Kolb R et al. Obesity-associated NLRC4 inflammasome activation drives breast cancer progression. *Nat. Commun.* 2016;7:13007.
28. Ohashi K et al. NOD-like receptor C4 Inflammasome Regulates the Growth of Colon Cancer Liver Metastasis in NAFLD. *Hepatology. Baltim. Md* 2019;70(5):1582–1599.

29. Verweyen E et al. Synergistic Signaling of TLR and IFN $\alpha/\beta$  Facilitates Escape of IL-18 Expression from Endotoxin Tolerance. *Am. J. Respir. Crit. Care Med.* 2020;201(5):526–539.
30. Van Der Kraak LA et al. Genetic and commensal induction of IL-18 drive intestinal epithelial MHCII via IFN $\gamma$ . *Mucosal Immunol.* 2021;14(5):1100–1112.
31. Gangur V, Simons FE, Hayglass KT. Human IP-10 selectively promotes dominance of polyclonally activated and environmental antigen-driven IFN-gamma over IL-4 responses. *FASEB J. Off. Publ. Fed. Am. Soc. Exp. Biol.* 1998;12(9):705–713.
32. Zumwalt TJ, Arnold M, Goel A, Boland CR. Active secretion of CXCL10 and CCL5 from colorectal cancer microenvironments associates with GranzymeB+ CD8+ T-cell infiltration. *Oncotarget* 2015;6(5):2981–2991.
33. Fuertes MB et al. Host type I IFN signals are required for antitumor CD8+ T cell responses through CD8 $\alpha$ + dendritic cells. *J. Exp. Med.* 2011;208(10):2005–2016.
34. Wennerberg E, Kremer V, Childs R, Lundqvist A. CXCL10-induced migration of adoptively transferred human natural killer cells toward solid tumors causes regression of tumor growth in vivo. *Cancer Immunol. Immunother.* 2015;64(2):225–235.
35. Borst J, Ahrends T, Bąbała N, Melief CJM, Kastenmüller W. CD4+ T cell help in cancer immunology and immunotherapy. *Nat. Rev. Immunol.* 2018;18(10):635–647.
36. Dodagatta-Marri E et al.  $\alpha$ -PD-1 therapy elevates Treg/Th balance and increases tumor cell pSmad3 that are both targeted by  $\alpha$ -TGF $\beta$  antibody to promote durable rejection and immunity in squamous cell carcinomas. *J. Immunother. Cancer* 2019;7(1):62.

37. Jiang Y, Zong W, Ju S, Jing R, Cui M. Promising member of the short interspersed nuclear elements (Alu elements): mechanisms and clinical applications in human cancers. *J. Med. Genet.* 2019;56(10):639–645.
38. Villa E, Ali ES, Sahu U, Ben-Sahra I. Cancer Cells Tune the Signaling Pathways to Empower de Novo Synthesis of Nucleotides. *Cancers* 2019;11(5):688.
39. Hu J, Ge H, Newman M, Liu K. OSA: a fast and accurate alignment tool for RNA-Seq. *Bioinformatics* 2012;28(14):1933–1934.
40. Love MI, Huber W, Anders S. Moderated estimation of fold change and dispersion for RNA-seq data with DESeq2. *Genome Biol.* 2014;15(12):550.
41. Ulgen E, Ozisik O, Sezerman OU. *pathfindR: An R Package for Pathway Enrichment Analysis Utilizing Active Subnetworks [Internet]*. Bioinformatics; 2018:
42. Kanehisa M, Furumichi M, Tanabe M, Sato Y, Morishima K. KEGG: new perspectives on genomes, pathways, diseases and drugs. *Nucleic Acids Res.* 2017;45(D1):D353–D361.
43. Newman AM et al. Robust enumeration of cell subsets from tissue expression profiles. *Nat. Methods* 2015;12(5):453–457.
44. Charoentong P et al. Pan-cancer Immunogenomic Analyses Reveal Genotype-Immunophenotype Relationships and Predictors of Response to Checkpoint Blockade. *Cell Rep.* 2017;18(1):248–262.
45. Li T et al. TIMER: A Web Server for Comprehensive Analysis of Tumor-Infiltrating Immune Cells. *Cancer Res.* 2017;77(21):e108–e110.

46. Hochberg Y, Benjamini Y. More powerful procedures for multiple significance testing. *Stat. Med.* 1990;9(7):811–818.

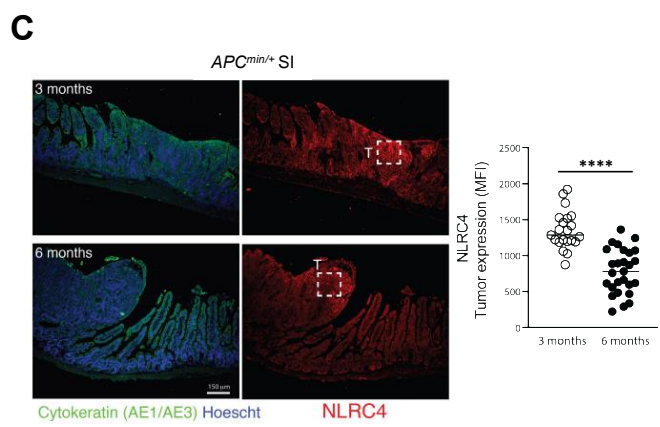
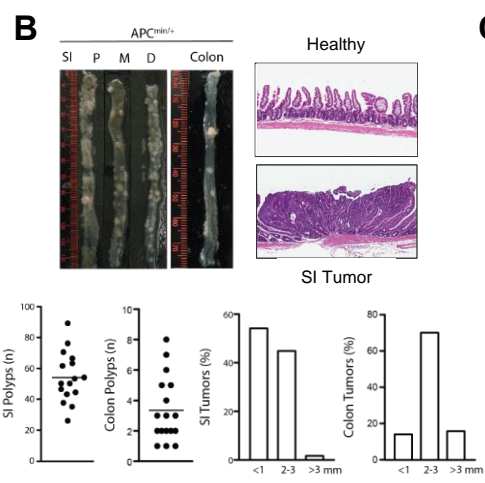
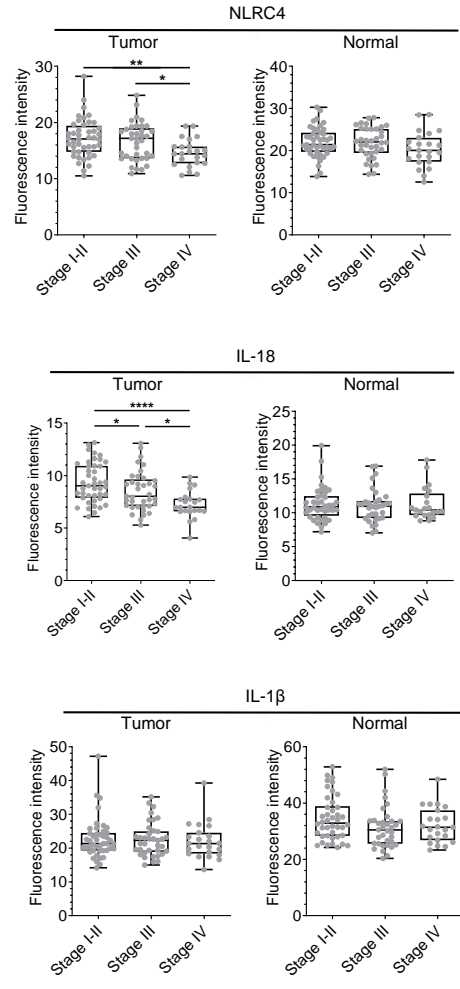
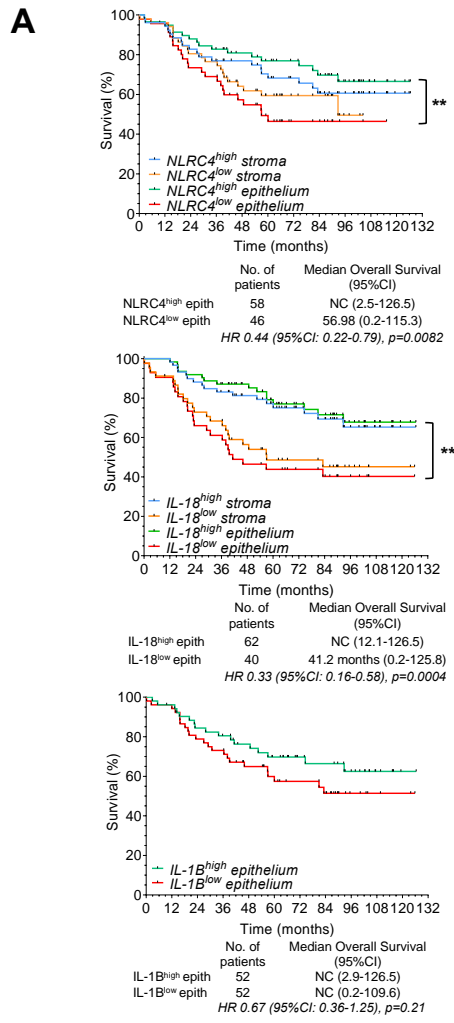
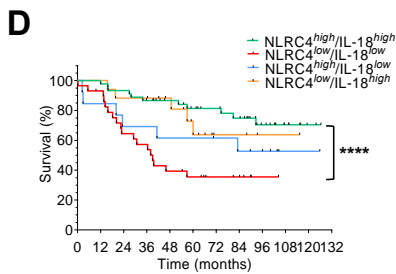
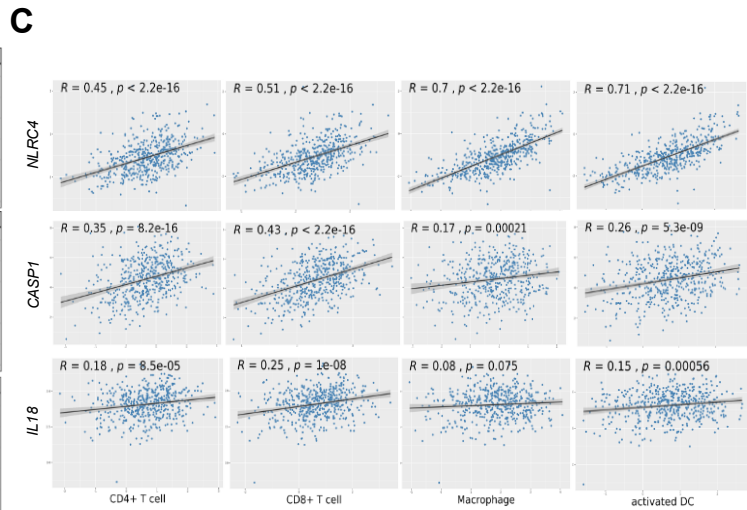
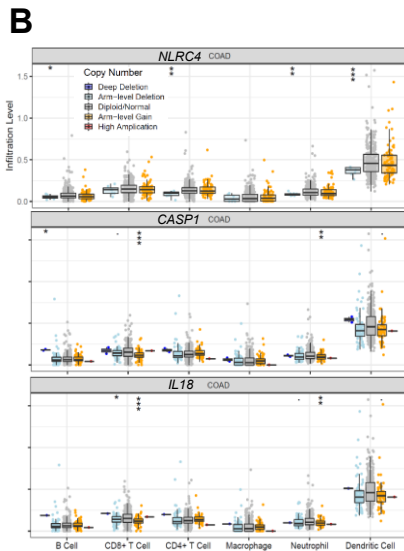
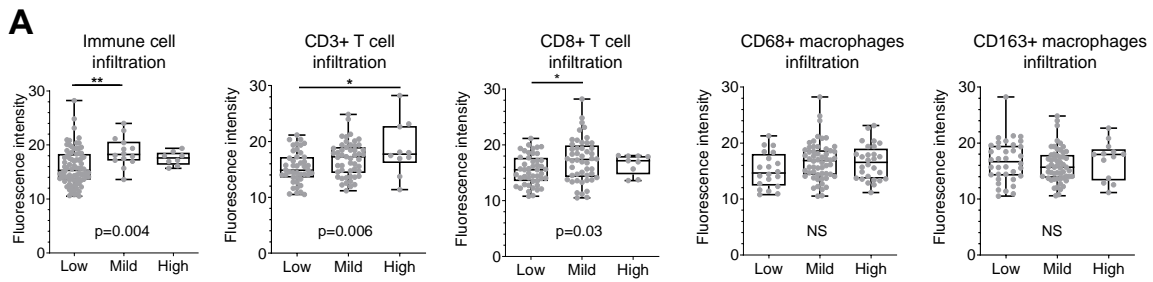


Figure 1

**Figure 1: Loss of tumor epithelial NLRC4 is associated to aggressive metastatic Stage IV, and decreased overall survival of colorectal cancer patients**

(A) To the left, association between protein expression levels of tumor epithelial NLRC4, IL-18, or IL-1 $\beta$ , with patient overall survival in the Bergonié Institute cohort. When available, patients were stratified based on protein expression levels of NLRC4, IL-1 $\beta$ , or IL-18, as high versus low expression in the colon epithelium (inside the cytokeratin mask) or in the stroma (outside the cytokeratin mask). 95%CI: 95% confidence interval; HR: Hazard Ratio. A log-rank test stratified according to protein expressions was used. NC: could not be calculated. Asterisks indicate p-values between high versus low expression of markers either inside or outside the mask. \*\*p<0.01; \*\*\*p<0.001. To the right, protein expression of tumor epithelial NLRC4, IL-18, or IL-1 $\beta$ , in various colorectal cancer tumor stages, classified in Stage I-II (localized), Stage III (locally advanced), and Stage IV (metastatic disease) (obtained from the Bergonié institute cohort). One-way ANOVA (parametric) or Kruskal-Wallis (non-parametric) tests were used to evaluate the significance of the differential expression between each disease stage. COAD, colon adenocarcinoma; READ, Rectum Adenocarcinoma; CHOL, cholangiocarcinoma; LUAD, lung adenocarcinoma; LUSC, lung squamous cell carcinoma. \*P<0.05, \*\*p<0.01, \*\*\*\*P<0.0001. (B) Top left, representative image of polyps of a 6 months old *Apc*<sup>Min/+</sup> mouse in the small intestine according to their position (P proximal, M middle or D distal) and in the colon; Top right, Hematoxylin and Eosin (H&E) of healthy small intestine and polyp-containing section of a 6 months old *Apc*<sup>Min/+</sup> mouse. (4X magnification). Bottom, quantification of the number of polyps in the SI of *Apc*<sup>Min/+</sup> mice (n=17); quantification of the number of polyps in the colon of *Apc*<sup>Min/+</sup> mice (n=17); the size distribution of polyps from 6 months old *Apc*<sup>Min/+</sup> mice in the SI and colon. (C) Representative immunofluorescence images of small intestine tissue sections at 3 or 6 months of *Apc*<sup>Min/+</sup> mice stained with anti-NLRC4 antibody (red). Cytokeratin (green) and Hoescht (blue) were used to stain epithelial cells and nuclear morphology, respectively. Insets correspond to boxed regions (150x150  $\mu$ m) used to quantify NLRC4 staining from tumor (T) portion of the tissue. Graph shows NLRC4 expression level (MFI) in tumor region of small intestine at 3 or 6 months of *Apc*<sup>Min/+</sup> mice. Data are mean +/- SEM of 21-27 distinct normal/tumor regions, 3 regions per mouse, 7-9 mice per time point. Statistical analysis was performed using student t-test (\*\*\*\*p<0.0001).



	No. of patients	Median Overall Survival (95%CI)
$NLRC4^{high}/IL-18^{high}$	45	NC (12.1-126.5)
$NLRC4^{high}/IL-18^{low}$	13	NC (2.5-125.8)
$NLRC4^{low}/IL-18^{high}$	17	NC (15.5-115.3)
$NLRC4^{low}/IL-18^{low}$	29	39.02 (0.2-104.4)

Population comparison		HR (95%CI, pvalue)
$NLRC4^{high}/IL-18^{high}$	$NLRC4^{low}/IL-18^{low}$	0.26 (0.09-0.45; $p=0.0001$ )
$NLRC4^{high}/IL-18^{high}$	$NLRC4^{high}/IL-18^{low}$	0.47 (0.12-1.31; $p=0.13$ )
$NLRC4^{high}/IL-18^{high}$	$NLRC4^{low}/IL-18^{high}$	0.67 (0.20-2.01; $p=0.44$ )
$NLRC4^{low}/IL-18^{high}$	$NLRC4^{low}/IL-18^{low}$	0.34 (0.17-0.88; $p=0.02$ )
$NLRC4^{high}/IL-18^{low}$	$NLRC4^{low}/IL-18^{low}$	0.60 (0.27-1.44; $p=0.27$ )

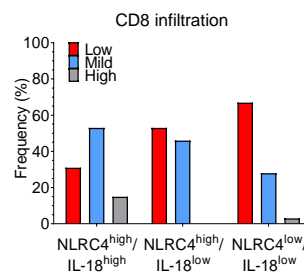
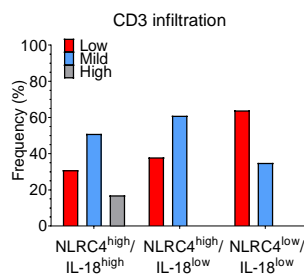
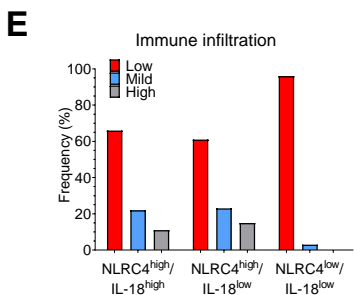
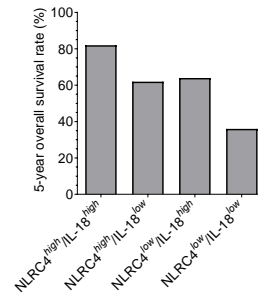


Figure 2

**Figure 2: Loss of tumor epithelial NLRC4 protein is associated with low tumor immune infiltration of CD3<sup>+</sup> T cells and activated DCs.** (A) Protein expression of tumor epithelial NLRC4 in various clinically defined levels of tumor total immune, total T cell, cytotoxic T cell, CD68<sup>+</sup> macrophage or CD163<sup>+</sup> macrophage infiltration; as determined by immunohistochemistry as low, medium, and high levels of infiltration in tumors (from the Bergonié Institute cohort). One-way ANOVA (parametric) or a Kruskal-Wallis test (non-parametric) were used to evaluate the correlation between expression intensity and levels of immune infiltrates. \*p<0.05; \*\*p<0.01. (B) Associations between *NLRC4*, *CASP1*, or *IL-18* somatic copy number alterations and composition of the tumor immune infiltrate, obtained from the TCGA cohort analysis and using TIMER software. Box plots are presented to show the distributions of each immune subset at each copy number status in COAD cancer patients. The infiltration level for each category is compared with the normal using two-sided Wilcoxon rank sum test. \*p<0.05; \*\*p<0.01; \*\*\*p<0.001. (C) Correlation coefficient and pvalues between *NLRC4*, *CASP1*, or *IL-18* transcripts and levels of immune infiltration for various immune cell subsets in COAD patients, obtained from the TCGA cohort and analysis using TIMER. (D) Association between protein expression levels of tumor epithelial NLRC4 and IL-18 with patient overall survival in the Bergonié Institute cohort. Patients were stratified based on protein expression levels of NLRC4 and IL-18 (to the left) as high versus low expression in the colon epithelium (inside the cytokeratin mask). 95%CI: 95% confidence interval; HR: Hazard Ratio. A log-rank test stratified according to protein expression was used. NC: could not be calculated. Asterisks indicate pvalues between pairs as indicated. \*\*\*\*p<0.0001. To the right, 5-year overall survival rate (%). (E) Frequency of patients with low, mild, or high tumor immune infiltrates (as pathologically characterized by immune infiltration, CD3<sup>+</sup> T cells, or CD8<sup>+</sup> T cells) among three different population of patients expressing high or low levels of tumor epithelial NLRC4 and/or IL-18 (from the Bergonié Institute cohort). COAD, colon adenocarcinoma.

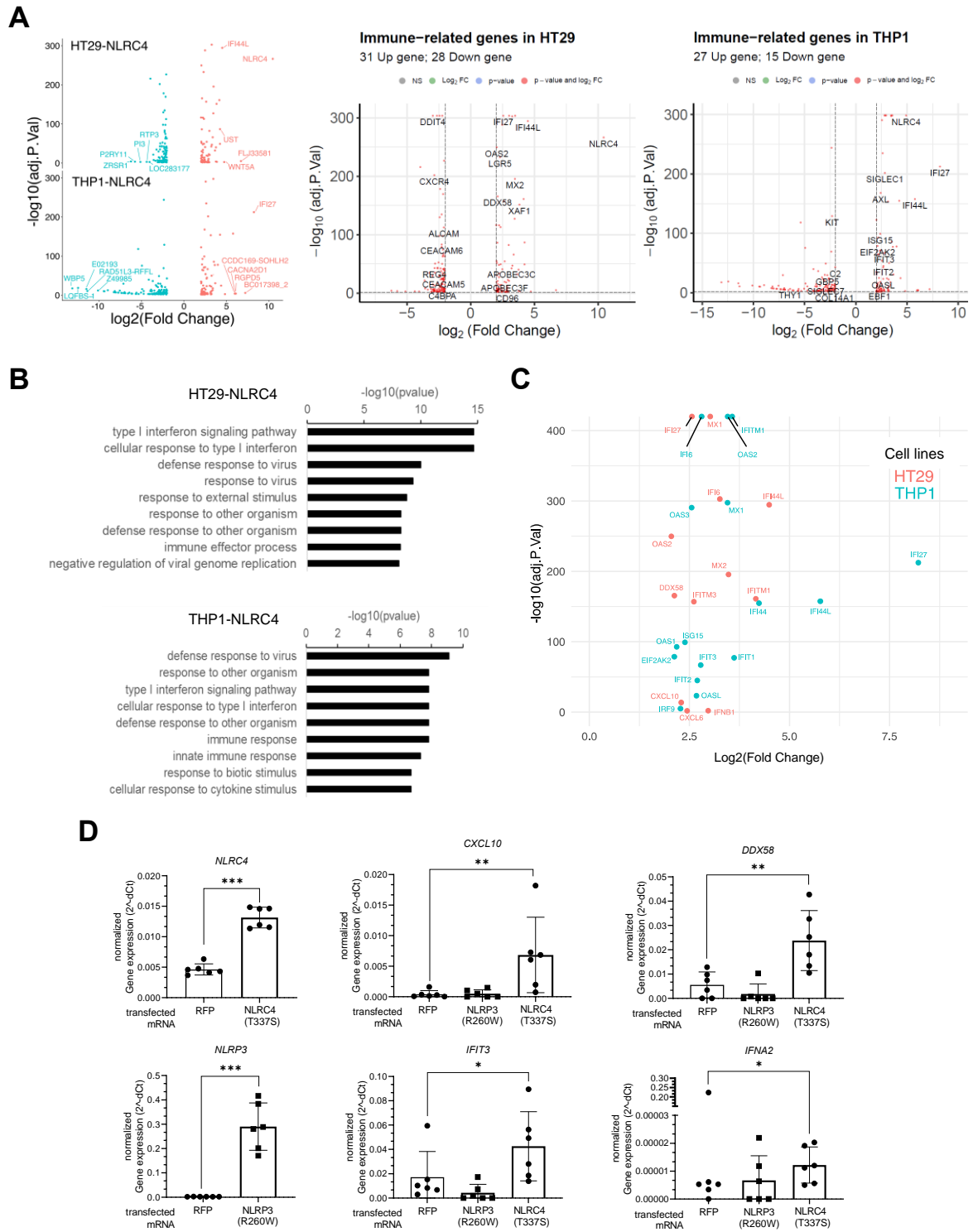


Figure 3

**Figure 3: NLRC4 expression in cancer cells triggers an immune transcriptional program.**

(A) To the left, volcano plots of differentially expressed genes in HT29-NLRC4 or THP1-NLRC4 versus mock control cell lines, as measured by RNAseq analysis. Differential gene expression performed with DeSeq2. X-axis shows the log<sub>2</sub>-transformed fold change of NLRC4-overexpressing lines over control, y-axis is the -log<sub>10</sub> transformation of the adjusted p-values. The 10 genes most downregulated (blue) or upregulated (red) are included. In the middle, volcano plots of differentially expressed immune-related genes in HT29-NLRC4 cell line; or to the right, in THP1-NLRC4 cell line. (B) Gene Ontology analysis using KEGG pathway of significant upregulated genes ( $p < 0.05$ ; FoldChange  $> 2$ ) in both NLRC4-expressing cell lines. (C) Dot plot representing NLRC4-induced Type I IFN genes from both cell lines (HT29-NLRC4, red; THP1-NLRC4, blue), with fold changes of gene expression and associated p-values. (D) mRNA transfections of NLRC4 (T337S), or NLRP3 (R260W), or control RFP, in human primary monocytes. Normalized gene expression levels by Q-PCR of *NLRC4* and *NLRP3* shown as control (left), or Type-I IFN genes induced by each mRNA transfection as indicated (right). Data as mean of two different donors pooled  $\pm$  SD (n=3 independent mRNA transfections per construct); all transfected constructs are compared to RFP control using Dunnett's test \* $p < 0.05$ ; \*\* $p < 0.01$ ; \*\*\* $p < 0.001$ .

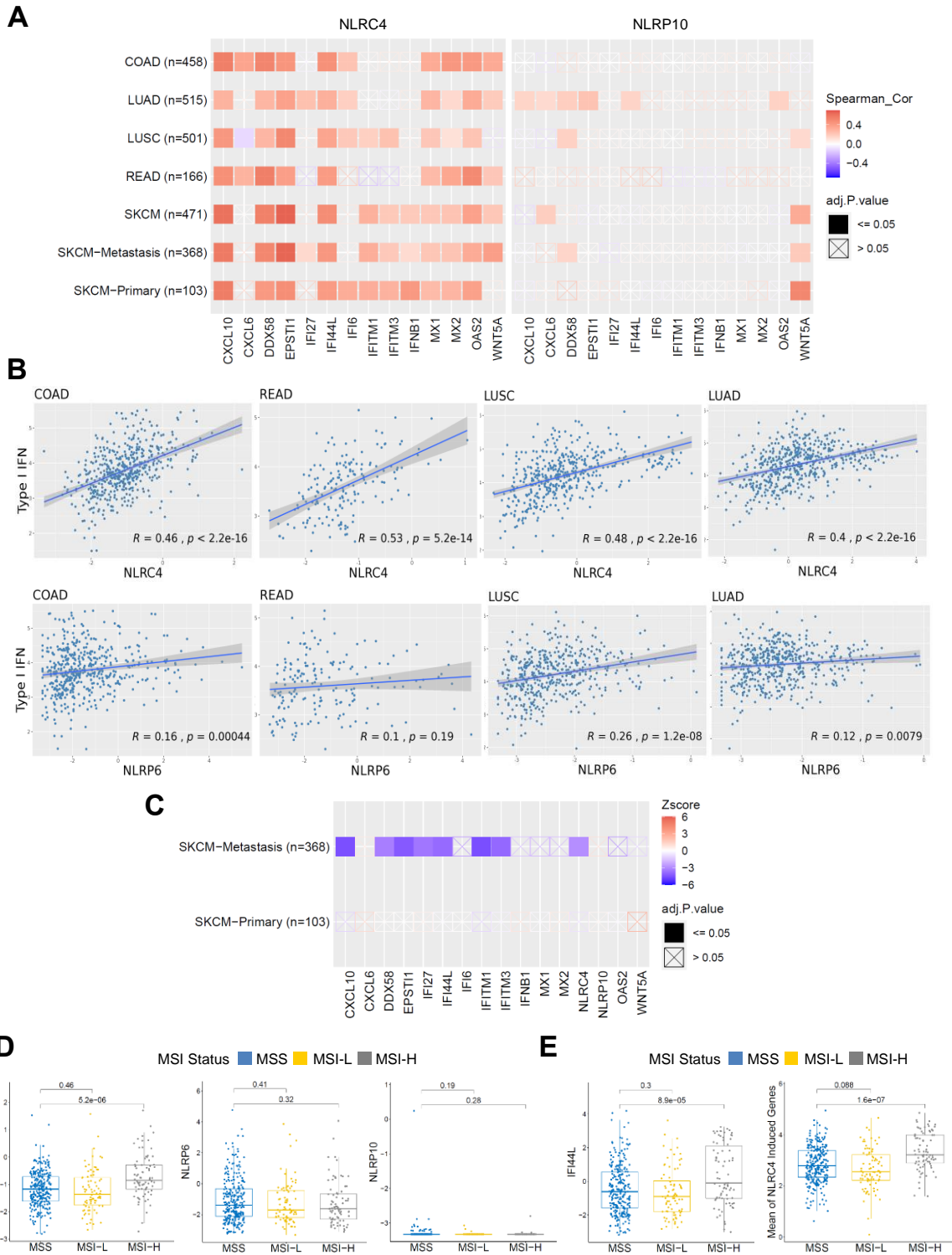


Figure 4

**Figure 4: *NLRC4* expression correlates with Type-I IFN gene signature, MSI<sup>high</sup> patient tumors, and is associated with decreased risk of metastasis.** (A) Correlation analysis between expression of the top Type-I IFN genes upregulated in HT29-NLRC4 cell line and *NLRC4* or *NLRP10*, in either colorectal cancer patients (COAD, READ), lung cancer patients (LUSC, LUAD), or skin cutaneous melanoma (SKCM, primary and metastasis). (B) Correlation analysis between expression of the broader Type-I IFN gene signature (see Methods) and *NLRC4* or *NLRP6* in colorectal cancer patients (COAD, READ), or in lung cancer patients (LUSC, LUAD). Patient datasets from the TCGA cohort; Spearman correlation coefficients R and pvalues are indicated (A, B). (C) Clinical outcome of the top Type-I IFN genes upregulated in HT29-NLRC4 cell line (including *NLRC4* or *NLRP10*) in SKCM primary versus metastasis. Patient datasets from the TCGA cohort; Zscores were determined by using TIMER2.0 and reflect clinical outcome for each gene (blue: decreased risk  $p < 0.05$ ,  $z < 0$ ; red: increased risk  $p < 0.05$ ,  $z > 0$ ), with adjusted pvalues indicated. (D) Association between gene expression of NLR-family members (*NLRC4*, *NLRP6* or *NLRP10*) and MSI status (E) Association between Type-I IFN genes (*IFI44L*, or the gene set encompassing the top 14 NLRC4-induced IFN genes from cell lines) and MSI status in COAD patient tumors. Patient datasets from the TCGA cohort, with adjusted pvalues indicated. Microsatellite instability (MSI) stable (MSS); Low (MSI-L); High (MSI-H). COAD, colon adenocarcinoma; READ, Rectum Adenocarcinoma; LUAD, lung adenocarcinoma; LUSC, lung squamous cell carcinoma.

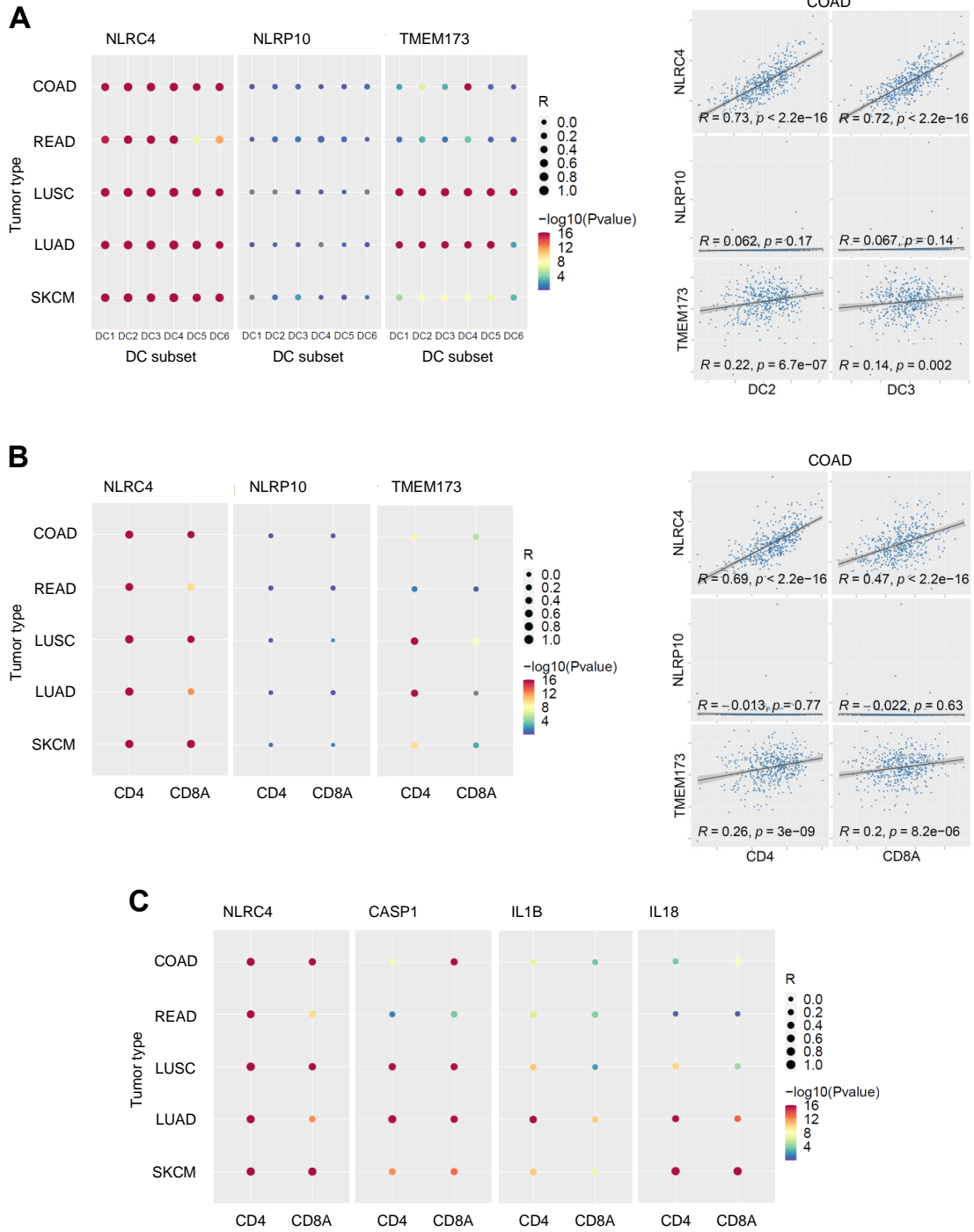


Figure 5

**Figure 5: *NLRC4* expression is associated to DC2/DC3s and CD4+/CD8+ T cell tumor infiltrates in cancer patients.** (A) To the left, expression correlation between *NLRC4*, *NLRP10*, or *TMEM173* (STING) and various tumor infiltrating DC subsets in colorectal (COAD, READ), or cancer patients (LUSC, LUAD), or melanoma SKCM. The various DC subset gene signatures used (for DC1, DC2, DC3, DC4, DC5, DC6) were obtained from scRNAseq of human blood. To the right, scatter plots showing correlation of gene expression between *NLRC4*, or *NLRP10*, or *TMEM173* and DC2 or DC3 gene signatures in COAD patient tumors. COAD datasets used were obtained from the TCGA cohort. (B) To the left, gene expression correlation between *NLRC4*, *NLRP10*, or *TMEM173* (STING) and CD4 or CD8A in patient tumors; correlation coefficient R is represented by the size of dot, log<sub>10</sub> (pvalue) is represented by the color of the dot. To the right, scatter plots showing correlation of gene expression between *NLRC4*, or *NLRP10*, or *TMEM173* and *CD4* or *CD8A* in COAD patient tumors. Correlation coefficients R and pvalues are indicated. (C) Gene expression correlation between *NLRC4*, *CASP1*, *IL1B*, or *IL18* and *CD4* or *CD8A* in patient tumors. For (A), (B), (C), data analysis was performed using the TCGA patient database cohort; correlation coefficients R are represented by the size of dot, Log<sub>10</sub> (pvalue) is represented by the color of the dot. COAD, colon adenocarcinoma; READ, Rectum Adenocarcinoma; LUAD, lung adenocarcinoma; LUSC, lung squamous cell carcinoma; SKCM, skin cutaneous melanoma.

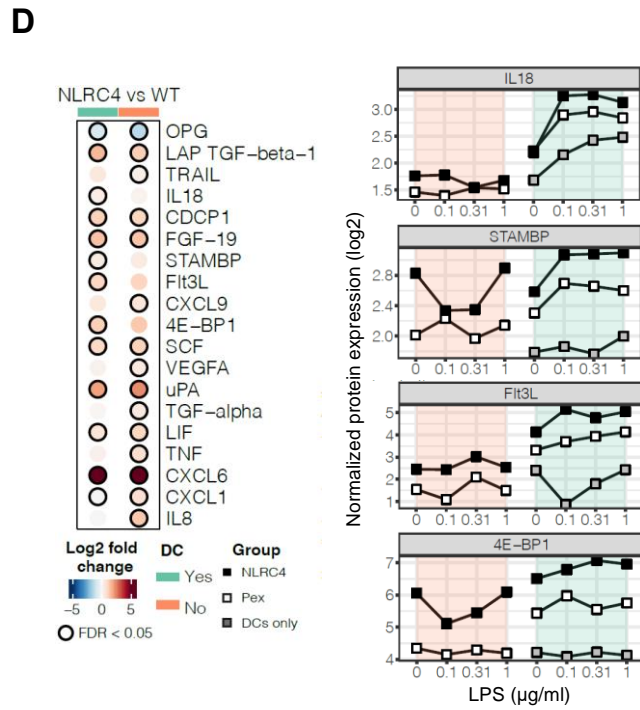
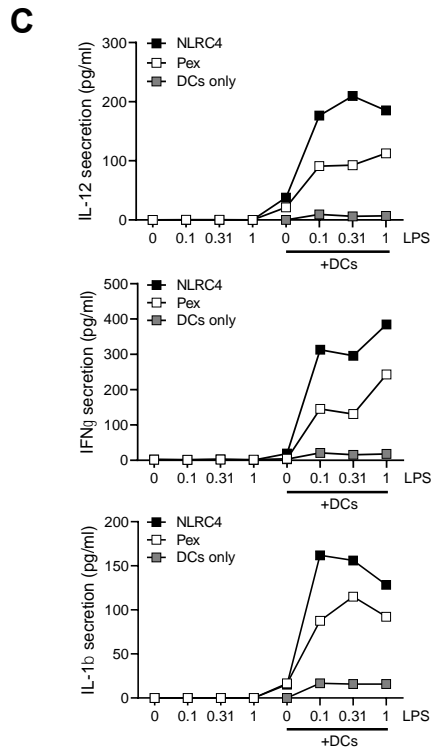
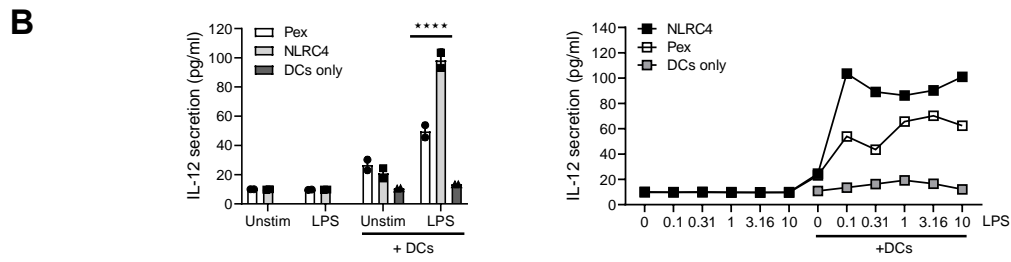
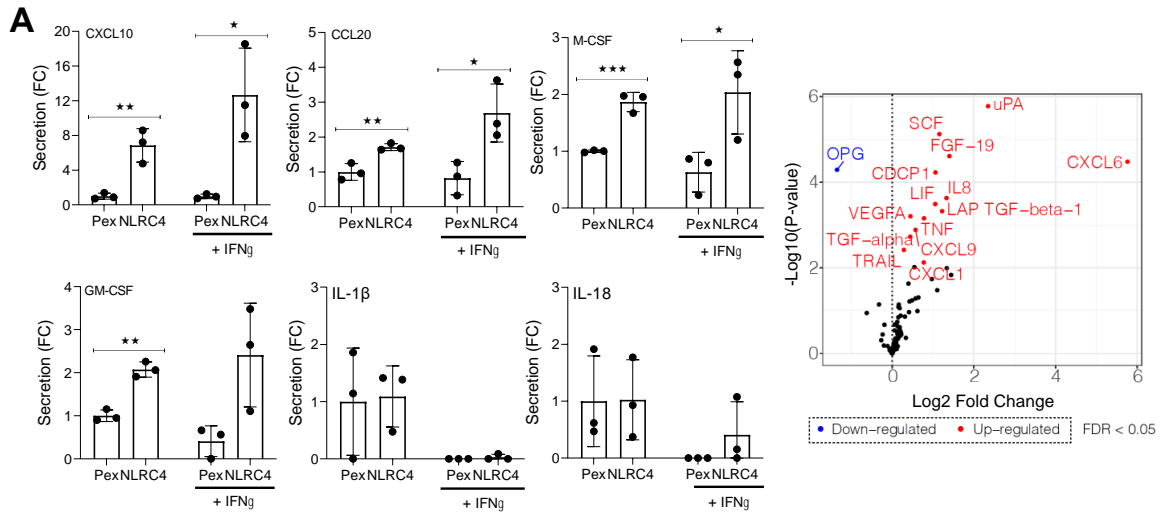


Figure 6

**Figure 6: NLRC4 expression in cancer cells mediates the release of Type-I IFN chemokines and myeloid growth factors to mature human primary DCs towards a Th1 immune response.** (A) To the left, HT29-NLRC4 cells or HT29-pEx control cells were cultured in Boyden chambers in the presence or not of IFN $\gamma$ , and release of the indicated immune mediators (chemokines, myeloid growth factors, cytokines) was measured from the top chamber by ELISA. To the right, volcano plot of differentially secreted proteins by HT29-NLRC4 versus mock control cell lines as measured by Olink proteomics. P-values were adjusted by multiple testing using Benjamini-Hochberg method (see Methods). (B) IL-12 secretion from cell culture supernatants measured by ELISA from cultures of HT29-NLRC4 cell line alone, HT29-pEx control cell line alone or either co-cultured with primary DCs isolated from human blood, with or without LPS (0.1 $\mu$ g/ml to the left, or various concentrations in  $\mu$ g/ml to the right). Co-cultures of HT29/DCs (1/1.2 ratio) were maintained for 24hrs, in the presence or not of LPS. (C) Same experiment as (B) but extended to a broader cytokine array as indicated by using MSD. Data as mean  $\pm$  SD (n=3), unpaired two tailed student t test \*P<0.05; \*\*P<0.01; \*\*\*P<0.001 (A). Data as mean  $\pm$  SD (duplicates), representative of 2 donors with similar pattern; 2way ANOVA Sidak test NLRC4 vs Pex \*\*\*\*P<0.0001 (B); Data representative of 2 donors with similar pattern (C). (D) Same experiment as in (B) but additional differentially secreted proteins as measured by Olink proteomics. Heatmap in the left panel indicates the log<sub>2</sub> fold changes between HT29-NLRC4 and WT cells (Pex control), in co-cultures with DCs (green) or not (orange) in the presence or not of LPS. Black circles indicate statistically significant changes after multiple testing. Plots to the right show the normalized protein expression values for the various markers, co-cultured or not with DCs, with or without LPS.